

NAVAL POSTGRADUATE SCHOOL
Monterey, California

1

AD-A281 644



DTIC
ELECTE
JUL 15 1994
S F D

94-22181



89/98

THESIS

**APPROXIMATION OF THE FAST BOTTOM
REFLECTION COEFFICIENT IN THE
QUADRUPLER EXPANSION OF THE METHOD
OF IMAGES IN A WEDGE SHAPED OCEAN**

by

Patrick Toyoki Takamiya

March 1994

Thesis Advisor:

A. B. Coppens

Approved for public release; distribution is unlimited

DTIC QUALITY INSPECTED 8

94 7 14 036

REPORT DOCUMENTATION PAGE			Form approved OMB No. 0704-188	
Public reporting burden for this collection of information is estimated to average 1 hour per response, including the time for reviewing instructions, searching existing data sources, gathering and maintaining the data needed, and completing and reviewing the collection of information. Send comments regarding this burden estimate or any other aspect of this collection of information including suggestions for reducing this burden, to Washington Headquarters services, Directorate for Information Operations and Reports, 1215 Jefferson Davis Highway, Suite 1204, Arlington, VA 22202-4302, and to the Office of Management and Budget, Paperwork Reduction Project (0704-0188), Washington, DC 20503.				
1. AGENCY USE ONLY (Leave Blank)		2. REPORT DATE	3. REPORT TYPE AND DATES COVERED	
		March 1994	Master's Thesis	
4. TITLE AND SUBTITLE			5. FUNDING NUMBERS	
Approximation of the Fast Bottom Reflection Coefficient in the Quadruplet Expansion of the Method of Images in a Wedge Shaped Ocean				
6. AUTHOR(S)				
Takamiya, Patrick Toyoki				
7. PERFORMING ORGANIZATION NAME(S) AND ADDRESS(ES)			8. PERFORMING ORGANIZATION REPORT NUMBER	
Naval Postgraduate School Monterey, CA 93943-5000				
9. SPONSORING/MONITORING AGENCY NAME(S) AND ADDRESS(ES)			10. SPONSORING/MONITORING AGENCY REPORT NUMBER	
11. SUPPLEMENTARY NOTES				
The views expressed in this thesis are those of the author and do not reflect the official policy or position of the Department of Defense or the U.S. Government				
12a. DISTRIBUTION/AVAILABILITY STATEMENT			12b. DISTRIBUTION CODE	
Approved for public release; distribution is unlimited.				
13. ABSTRACT (Maximum 200 words)				
Image theory is an ideal method for calculating the transmission loss in a shallow water (wedge shaped ocean) environment. It can be used in cross-slope, at all frequencies and in transitional cut off regions that are out of bounds to normal mode theories.				
This thesis had three objectives: 1) convert the existing image theory models called URTEXT and WEDGE into a high level scripting language called MATLAB™ by Math Works, 2) linearize the existing quadruplet expansion program to increase speed, and 3) to incorporate the Arctan approximation of the Rayleigh reflection coefficient into the quadruplet expansion for the fast bottom case.				
Objective 1 was completed with accurate results. Objective 2 was completed with a factor of 8 increase in speed. Objective 3 incorporated the Arctan approximation of the reflection coefficient for a fast bottom into the quadruplet expansion, but due to the inaccuracy of the reflection coefficient after the second quadruplet, the results were not favorable. It was also discovered that even with the Rayleigh reflection coefficient, the first order approximations made in developing the quadruplet expansion equation (Equation 6-27) are not accurate enough for the fast bottom case.				
14. SUBJECT TERMS			15. NUMBER OF PAGES	
Acoustic Models, Computer Models, Method of Images, Quadruplet Expansion			89	
			16. PRICE CODE	
17. SECURITY CLASSIFICATION OF REPORT	18. SECURITY CLASSIFICATION OF THIS PAGE	19. SECURITY CLASSIFICATION OF THIS ABSTRACT	20. LIMITATION OF ABSTRACT	
Unclassified	Unclassified	Unclassified	UL	

Approved for public release; distribution is unlimited.

**Approximation of the Fast Bottom Reflection Coefficient in the Quadruplet
Expansion of the Method of Images in a Wedge Shaped Ocean**

by

**Patrick Toyoki Takamiya
Lieutenant, United States Navy
B.S.C.E., Purdue University, 1987**

Submitted in partial fulfillment of the requirements for
the degree of

MASTER OF SCIENCE IN APPLIED SCIENCE

from the


**NAVAL POSTGRADUATE SCHOOL
March 1994**

Author:


Patrick Toyoki Takamiya

Approved by:


Alan B. Coppens, Thesis Advisor


James V. Sanders, Second Reader


J. N. Eagle, Chairman Undersea Warfare Group

ABSTRACT

Image theory is an ideal method for calculating the transmission loss in a shallow water (wedge shaped ocean) environment. It can be used in cross-slope, at all frequencies and in transitional cut off regions that are out of bounds to normal mode theories.

This thesis had three objectives: 1) convert the existing image theory models called URTEXT and WEDGE into a high level scripting language called MATLAB™ by Math Works, 2) linearize the existing quadruplet expansion program to increase speed, and 3) to incorporate the Arctan approximation of the Rayleigh reflection coefficient into the quadruplet expansion for the fast bottom case.

Objective 1 was completed with accurate results. Objective 2 was completed with a factor of 8 increase in speed. Objective 3 incorporated the Arctan approximation of the reflection coefficient for a fast bottom into the quadruplet expansion, but due to the inaccuracy of the reflection coefficient after the second quadruplet, the results were not favorable. It was also discovered that even with the Rayleigh reflection coefficient, the first order approximations made in developing the quadruplet expansion equation (Equation 6-27) are not accurate enough for the fast bottom case.

Accession For	
NTIS CRA&I	<input checked="checked" type="checkbox"/>
DTIC TAB	<input type="checkbox"/>
Unannounced	<input type="checkbox"/>
Justification	
By	
Distribution /	
Availability Codes	
Dist	Avail and/or Special
A-1	

TABLE OF CONTENTS

I. INTRODUCTION.....	1
A. PARABOLIC EQUATION	1
B. NORMAL MODE THEORY	2
C. IMAGE THEORY.....	3
II. IMAGE THEORY.....	5
III. DOUBLET FORMATION	12
A. GENERAL DESCRIPTION.....	12
B. DEVELOPMENT	13
1. Balanced Doublet.....	14
2. Unbalanced Doublet	16
3. Distance from Doublet to Receiver.....	17
4. Pressure from Each Doublet	18
IV. QUADRUPLLET FORMATION.....	19
A. QUADRUPLLET GENERAL DESCRIPTION	19
B. QUADRUPLLET DEVELOPMENT	20
1. Balanced Quadruplet.....	20
2. Unbalanced Quadruplet	20
V. REFLECTION COEFFICIENTS.....	24
A. REFLECTION COEFFICIENTS.....	24
B. SLOW BOTTOM REFLECTION COEFFICIENTS.....	25
C. FAST BOTTOM REFLECTION COEFFICIENTS	27
VI. GRAZING AND RECEIVER ANGLES IN QUADRUPLLET	30
A. RECEIVER ANGLE	30

B. ANGLE OF INCIDENCE FOR UPPER AND LOWER DOUBLET IMAGES	32
C. AMPLITUDES	33
VII. PROCEDURE AND RESULTS.....	36
A. CONVERT WEDGE/URTEXT TO MATLAB.....	36
B. LINEARIZATION OF QUADRUPLLET EXPANSION PROGRAM.....	46
C. FAST BOTTOM REFLECTION COEFFICIENT APPROXIMATION	47
VIII. CONCLUSION AND RECOMMENDATIONS	53
APPENDIX A-1.....	54
APPENDIX A-2.....	57
APPENDIX B-1	60
APPENDIX B-2.....	65
LIST OF REFERENCES.....	70
BIBLIOGRAPHY	73
DISTRIBUTION LIST.....	76

LIST OF TABLES

TABLE 7-1 SLOW BOTTOM COMPARISON OF URTEXT AND WEDGEMATTR.....	38
TABLE 7-2 SLOW BOTTOM COMPARISON OF URTEXT AND WEDGEMATTR.....	39
TABLE 7-3 SLOW BOTTOM COMPARISON OF URTEXT AND WEDGEMATTR.....	40
TABLE 7-4 SLOW BOTTOM COMPARISON OF URTEXT AND WEDGEMATTR.....	41
TABLE 7-5 FAST BOTTOM COMPARISON OF WEDGE AND WEDGEMATTR WITH BOTTOMLOSS	42
TABLE 7-6 FAST BOTTOM COMPARISON OF WEDGE AND WEDGEMATTR WITH BOTTOMLOSS	43
TABLE 7-7 FAST BOTTOM COMPARISON OF WEDGE AND WEDGEMATTR IN CROSS-SLOPE WITH BOTTOMLOSS	44
TABLE 7-8 FAST BOTTOM COMPARISON OF WEDGE AND WEDGEMATTR IN CROSS-SLOPE WITH BOTTOMLOSS	45
TABLE 7-9 EXECUTION TIME OF IMAGE PROGRAMS.....	46
TABLE 7-10 COMPARISON OF RAYLEIGH AND ARCTAN APPROXIMATION REFLECTION COEFFICIENTS.....	48
TABLE 7-11 COMPARISON OF THE CUMULATIVE RAYLEIGH AND ARCTAN APPROXIMATION REFLECTION COEFFICIENTS.....	49

TABLE 7-12 COMPARISON OF AMPLITUDE AND PHASE OF USING RAYLEIGH AND ARCTAN APPROXIMATION.....	51
TABLE 7-13 COMPARISON OF AMPLITUDE AND PHASE OF QUADRUPLLET EXPANSION USING RAYLEIGH AND IMAGE MODEL.....	51

LIST OF FIGURES

Figure 2-1 - Wedge Geometry	5
Figure 2-2 - Image Structure for Wedge Shaped Duct.....	6
Figure 2-3 - Source-Receiver Geometry (Upper Image).....	7
Figure 2-4 - Comparison of Real and Image Theory Sound Propagation Paths.....	8
Figure 2-5 - Incident Angle θ_{nm} Calculation (Upper Half Space).....	9
Figure 3-1 - Doublet Image Structure.....	12
Figure 3-2 - Doublet Close-Up.....	14
Figure 3-3 - Geometry of Neutral Doublet.....	15
Figure 3-4 - Geometry of Unbalanced Doublet.....	16
Figure 3-5 - Doublet Three Dimensional Geometry.....	17
Figure 4-1 - Quadruplet Illustration.....	19
Figure 4-2 - Illustration of Unbalanced Quadruplet Amplitude.....	21
Figure 4-3 - Illustration of Δr in a Quadruplet.....	22
Figure 5-1 - Typical Fast Bottom Cumulative Reflection Coefficient Curve.....	28
Figure 6-1 - Grazing and Receiver Angles for Upper Doublet.....	31
Figure 7-1 - Pressure vs. Receiver Angle.....	37
Figure 7-2 - Comparison of Complex Reflection Coefficients.....	49

LIST OF SYMBOLS

A_n	-	amplitude of the nth doublet or upper doublets in a quadruplet
B_n	-	amplitude of the nth lower doublet in a quadruplet
b	-	ratio of densities of the bottom to water (ρ_2/ρ_1)
c	-	ratio of speed of sound of bottom to water (c_2/c_1)
c_1	-	speed of sound in seawater
c_2	-	speed of sound in bottom material
d	-	vertical distance between image doublets
k_n	-	wavenumber for n number modes
n	-	image number
P_n	-	pressure contribution by the nth doublet or quadruplet
P	-	total pressure
P_l	-	sum of complex partial pressures of the lower half-space
P_u	-	sum of complex partial pressures of the upper half-space
R_n	-	cumulative reflection coefficient of the nth image
R_{nm}	-	reflection coefficient of the nth image from the mth plane
r	-	distance from midpoint of the neutral doublet to the receiver
r_1	-	distance from apex to source
r_2	-	distance from apex to receiver
r_{n+}	-	distance from the nth image or midpoint of the nth doublet to the receiver in the upper image plane
r_{n-}	-	distance from the nth image or midpoint of the nth doublet to the receiver in the lower image plane
X_c	-	scaling distance for fast bottom

X_S	-	scaling distance for slow bottom
x	-	ratio of the sine of nth image going through the mth plane to the sine of the critical angle measured from the horizontal $\frac{\sin(\theta_{nm})}{\sin(\theta_c)}$
y_0	-	distance along the shore between the receiver and source
α	-	$\frac{2bc}{\sqrt{1-c^2}}$
α/k_2	-	bottom loss coefficient
β	-	wedge angle
γ	-	source angle measured downward from the surface
ΔA	-	difference in amplitude of upper and lower image in a doublet or upper and lower image doublet in a upper half-space in a quadruplet
ΔB	-	difference in amplitude in upper and lower image doublet in lower half-space in a quadruplet
Δr	-	difference in distance of the upper and lower image as compared to the midpoint in a doublet
δ	-	receiver angle measured downward from the surface
ρ_1	-	density of seawater
ρ_2	-	density of bottom material
θ_c	-	critical angle for fast bottom ($c_2 > c_1$)
θ_s	-	'critical angle' for slow bottom ($c_1 < c_2$), $\cos^{-1}(c_2 / c_1)$
θ_n		grazing angle of the nth image above or below the bottom
θ_{nm}	-	grazing angle of the nth image passing through the mth plane
θ_{no}	-	angle of incidence for nth image with virtual bottom wrt the surface
$\theta_{n\pm}$	-	angle of incidence for nth doublet midpoint wrt the surface
$\theta_{n+\pm}$	-	angle of incidence for the nth upper doublet, upper and lower images wrt the surface

$\theta_{n,\pm}$.	angle of incidence for the nth lower doublet, upper and lower images wrt the surface
$\epsilon_{n\pm}$.	receiver angle from nth upper and lower doublet midpoints
$\epsilon_{n+\pm}$.	receiver angle from the nth upper doublet upper and lower images
$\epsilon_{n-\pm}$.	receiver angle from the nth lower doublet upper and lower images
μ	-	$\frac{r_2}{ r_1 - r_2 }$
ϕ	-	$kr_1\mu(1 - \cos(2n\beta))$

ACKNOWLEDGMENT

I want to express my deepest appreciation to God and give Him all the glory as He has pointed me in the right direction and given me the tools to successfully achieve all tasks put before me.

I thank my wife Ginger, and sons Patrick, Darth, and Hunter for their patience, encouragement, and endurance of the long hours of study and thesis work.

I wish to thank Dr. David Kast, Gretchen, Pastor Murray, Pastor P.J. Sawyer, and Pastor John Wynn for their timely messages from the pulpit and encouragement over the last 18 months. Your leadership by example will leave an indelible mark in my spiritual life. I would also like to thank the members of Seaside Assembly of God and On Guard Youth Ministries for making Monterey such a wonderful experience.

Finally, I would like to thank my mother, Tomiko, for raising me with the discipline and work ethic that was so instrumental to completing this work.

I. INTRODUCTION

The current emphasis of undersea warfare is on the shallow coastal regions in littoral waters. The sound propagation in these regions is influenced by bottom and surface interaction and not by the convergence zones and ducting found in deep water. The variables in shallow water are bottom type, bottom density, slope, sea state, surface winds, sea surface temperature, etc., all of which can change quickly or be unavailable in the area of interest.

There is no closed form analytic solution to the problem of a penetrable, sloping bottom as found on the continental shelf region or shoreline areas. There are computer models using various approximation methods ranging from purely numerical (parabolic equation) to approximately analytical (adiabatic mode theory). Transmission loss modeling in a wedge shaped ocean falls into three major areas: 1) parabolic approximation, 2) adiabatic normal mode theory, and 3) image theory.

A. PARABOLIC EQUATION

The parabolic equation (PE) is a range-dependent, underwater acoustic propagation model. In it the Helmholtz equation is replaced by a one-way parabolic equation which generates an acoustic field as an initial value problem. The PE approach is limited by excessive computer running time in shallow water environments, higher frequencies, and horizontal rays $< 40^\circ$.

The first application of PE to underwater acoustics was by Tappert in 1977 with a restriction on the maximum angular aperture of $\pm 20^\circ$ at the source [Ref. 1]. This restriction was relaxed to $\pm 40^\circ$ with a higher order parabolic equation by Collins [Ref. 2]. Computerized calculations by Jensen and Kuperman [Ref. 3] based on a split-step Fast

Fourier Transform (FFT) solution of the parabolic equation provided detailed information about the beams projected into the bottom, showing modal cutoffs. The results compared favorably to model tank experiments by Coppens and Sanders [Ref. 4]. Since the PE is cylindrically symmetric, sloping bottoms cause a problem. Lee and McDaniel [Ref. 5] sectioned the wedge into a series of range independent regions and then applied normal PE methods. Another approach to this problem is by Collins [Ref. 6] with the rotated PE. The rotated PE steps parallel to the ocean bottom and has two normal derivatives preserving pressure and particle velocity normal components thus handling sloping interfaces properly. Fawcett [Ref. 7] developed a three-dimensional computer model using the wide-angle PE approximation by Thomson [Ref. 8] with FFT algorithm as an azimuthal operator. Most recently, Collins [Ref. 9] has developed the energy conserving PE for elastic media to improve accuracy in range-dependent elastic media. The energy-conserving elastic PE is a generalization of the energy conserving acoustic PE [Ref. 10]. It involves approximating a range-dependent waveguide into a sequence of range-independent regions with a linear approximation of compressional energy flux between the vertical interfaces.

B. NORMAL MODE THEORY

Normal mode theory provides an exact solution to the wave equation. The distinct advantage of normal modes is that once the set of eigenfunctions have been determined, the range and depth dependence of the transmission loss can be calculated directly [Ref. 11].

Normal mode theory is a range-independent approach but for a wedge shaped ocean, a range-dependent approach is needed due to the bottom interaction (in the case of a lossy bottom) and bottom reflection angle. Pierce [Ref. 12] used adiabatic separation of depth and range in the wave equation to get an approximation. Graves, Nagl, Uberall, and Zarur [Ref. 13] applied this method to the wedge shaped ocean using rigid bottom and isospeed

water. This method was good only for small slopes. Buckingham [Ref. 14] developed a solution for the penetrable bottom using an "effective" wedge with pressure release bottom below the actual penetrable bottom. By using a coordinate transformation, range-dependent modes are matched to range independent eigenfunctions in the "effective" wedge to account for amplitude and phase shifts. Then a sum of range dependent normal modes are applied to the new bottom.

A problem with adiabatic normal mode approximation is it does not explain the transition to evanescent modes at cutoff. Pierce [Ref. 15] combined PE with adiabatic normal mode theory to develop a critical depth function. Known as the augmented adiabatic mode theory, it is a sum of modal terms with each mode eventually encountering a critical depth at a critical range. The results compare well with the results of Jensen and Kuperman [Ref. 3].

Another method is to combine local modes with ray acoustics. Arnold and Felsen [Ref. 16] developed intrinsic wave functions that are determined by waveguide geometry. Modes are mutually decoupled thus propagate independent of source geometry (physical shape) when superpositioned.

C. IMAGE THEORY

Image theory in acoustics is similar to image theory in optics. A source radiating in the water has a virtual image reflected equidistant above the water 180° out of phase. In an isospeed, wedge shaped ocean numerous images are produced in kaleidoscope fashion.

In 1966, Macpherson and Dainteth [Ref. 17] proposed a phase incoherent model for upslope propagation. Kawamura and Ioannou [Ref. 18] predicted the pressure amplitude and phase of the sound field along the bottom of a wedge shaped fluid layer overlapping a fast fluid bottom. Coppens, Humphries, and Sanders [Ref. 19] developed a phase coherent model to calculate the pressure amplitude along the bottom of a wedge of water overlying a

fast fluid bottom in the upslope direction using the incident plane wave reflection coefficient stated by Rayleigh. The pressure distribution at the water-bottom interface can be used as a source to project beams into the bottom to calculate the propagation through the medium. Brekhovskikh and Lysenov [Ref. 20] stated that for very distant source and image combinations or the presence of many reflections allow image theory to be applied with Rayleigh reflection coefficients with insignificant error. Baek [Ref. 21] then developed a computer model of pressure throughout the water column over a fast bottom. This model was limited to a fast bottom due to the critical grazing angle of the sound to bottom. LeSesne [Ref. 22] used the same model as a basis for a three-dimensional model which produced a pressure field in the cross slope case which was validated against experimental results from a model tank by Kosnick [Ref. 23]. Kaswandi [Ref. 24] developed a model for a pressure field with a slow bottom in downslope. Nassopoulos [Ref. 25] took all previous models developed at the Naval Postgraduate School and combined them into a computer program called URTEXT. He also implemented the use of the doublet expansion of the acoustic field in a wedge shaped ocean. Livingood [Ref. 26] then expanded the image doublets into the cross-slope case. Joyce [Ref. 27] then developed the quadruplet expansion of the acoustic pressure field in the wedge shaped ocean. The quadruplet expansion is a much faster computationally but the approximations in the reflection coefficient and other terms in the quadruplet expansion equation produces large errors at large wedge ($\beta > 3^\circ$) and source angles due to the angular differences between the images in the upper and lower doublets.

II. IMAGE THEORY

This section is a brief review of the ideas and basic equations of image theory. The following assumptions are made:

1. Sound velocities and densities are constant in both the wedge and penetrable bottom.
2. Air-water boundary is a pressure release surface i.e. reflections are 180° out of phase.
3. Slope is constant and all boundaries are planar.

When sound is transmitted within a waveguide, there are a number of interactions of the acoustic waves with the boundaries. In image theory, each ray path is replaced by an image of the source. The distance of the source from the receiver is the total length of the acoustic ray. In the case of a sloping bottom, the image is placed equidistant from the reflecting boundary perpendicular from the source. See Figure 2-1.

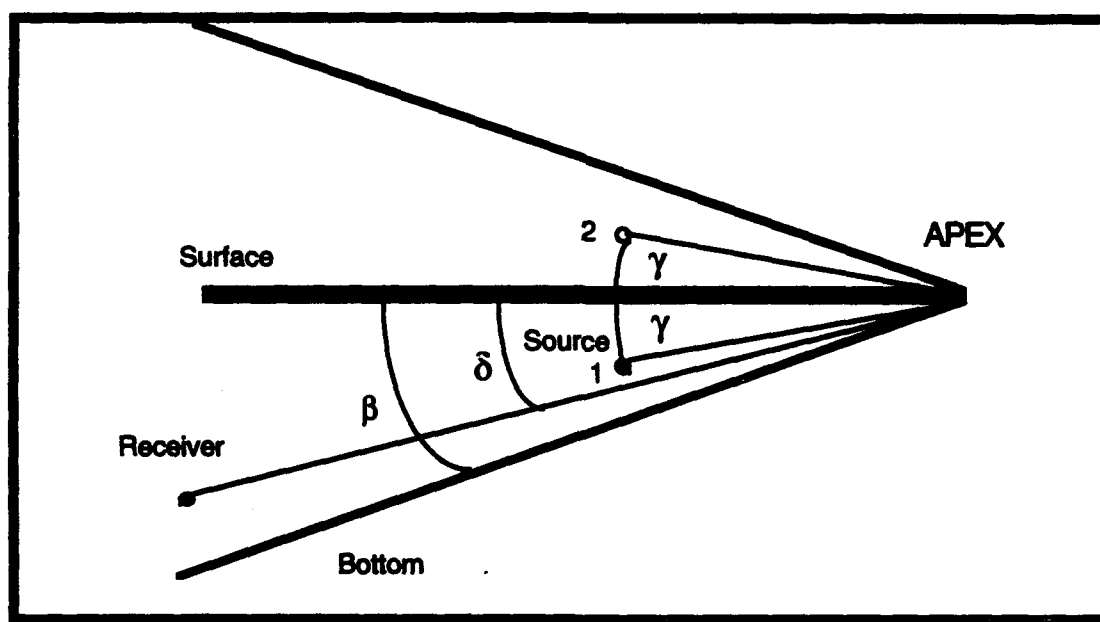


Figure 2-1 -Wedge Geometry

For a given bottom slope angle β , the number of images N in each of the upper and lower half spaces is given by

$$N = \text{Int}\left(\frac{180}{\beta}\right) \quad (2-1)$$

Each image is numbered from the source. The source is image number 1 for the upper half space. The first image below the bottom is image number 1 for lower half space. This is continued until the opposite surface is reached. See Figure 2-2.

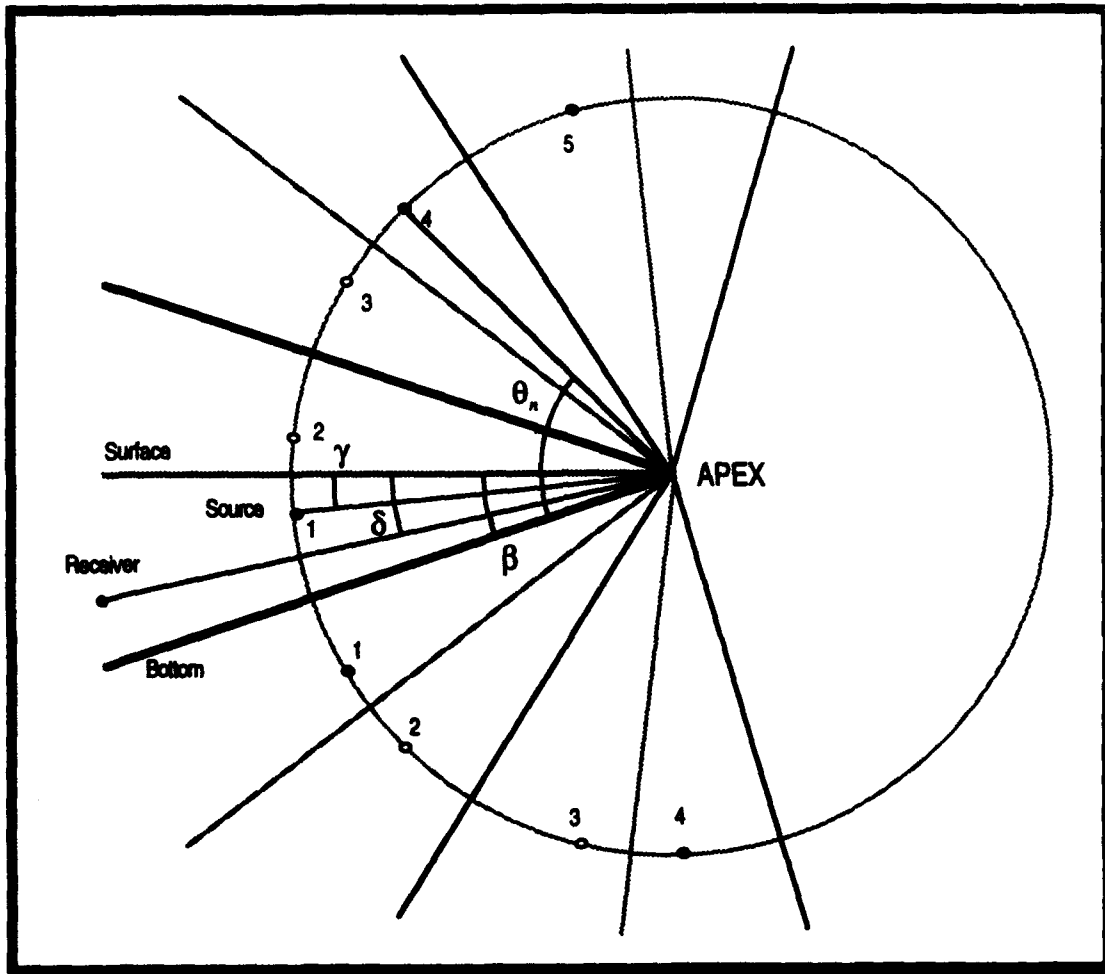


Figure 2-2 - Image Structure for Wedge Shaped Duct

The grazing angle θ_n of the n th image above or below the bottom is calculated from

$$\theta_n = n\beta - \gamma \quad \text{for } n \text{ odd} \quad (2-2)$$

$$\theta_n = (n-1)\beta + \gamma \quad \text{for } n \text{ even} \quad (2-3)$$

where γ is the angle of the source from the surface.

The range r_n from each image to the receiver is then calculated using

$$r_{n+} = \sqrt{r_1^2 + r_2^2 + y_0^2 - 2r_1r_2 \cos(\theta_n - \beta + \delta)} \quad (2-4)$$

for the upper series of images and

$$r_{n-} = \sqrt{r_1^2 + r_2^2 + y_0^2 - 2r_1r_2 \cos(\theta_n + \beta - \delta)} \quad (2-5)$$

for the lower series of images. In these equations, r_1 is the distance from the wedge apex to the source, r_2 is the distance from the apex to the receiver, y_0 is the cross-slope or shoreline distance between the source and receiver, and $\theta_n - \beta + \delta$ is the angle from the n th source to the receiver (for the upper image). See Figure 2-3.

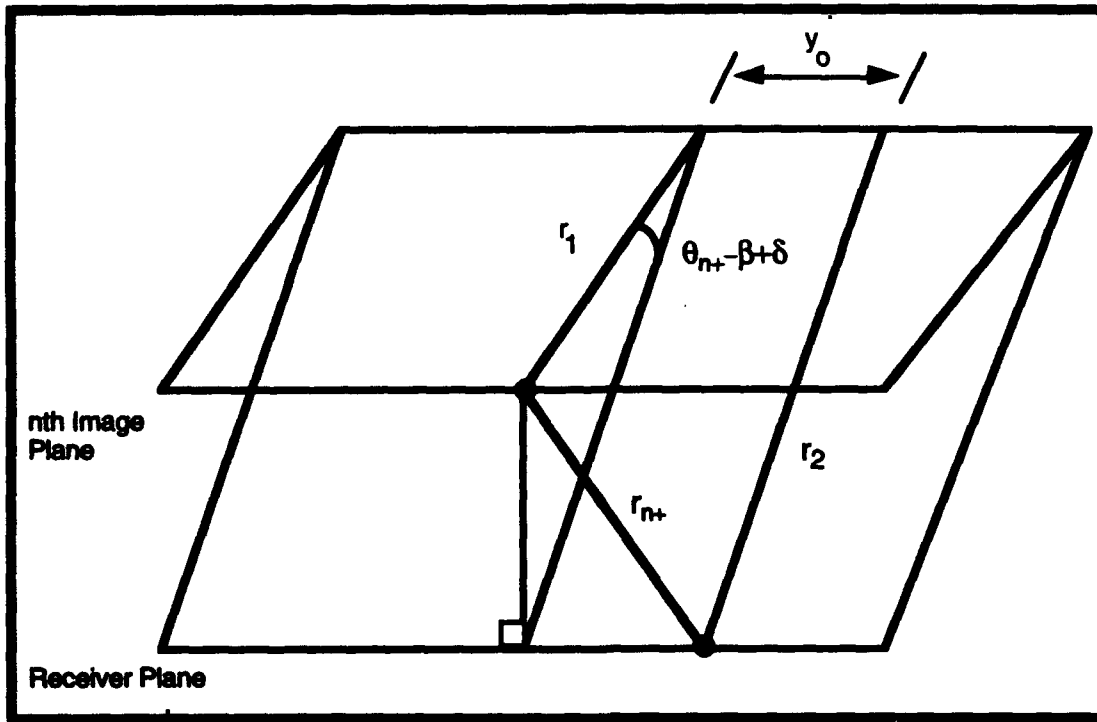


Figure 2-3 - Source-Receiver Geometry (Upper Image)

The sound will propagate from the source to the receiver through combinations of three different path types: 1) direct, 2) surface reflected, and 3) bottom reflected. Figure 2-4 illustrates a bottom-surface-bottom path. The upper drawing illustrates the real path of sound.

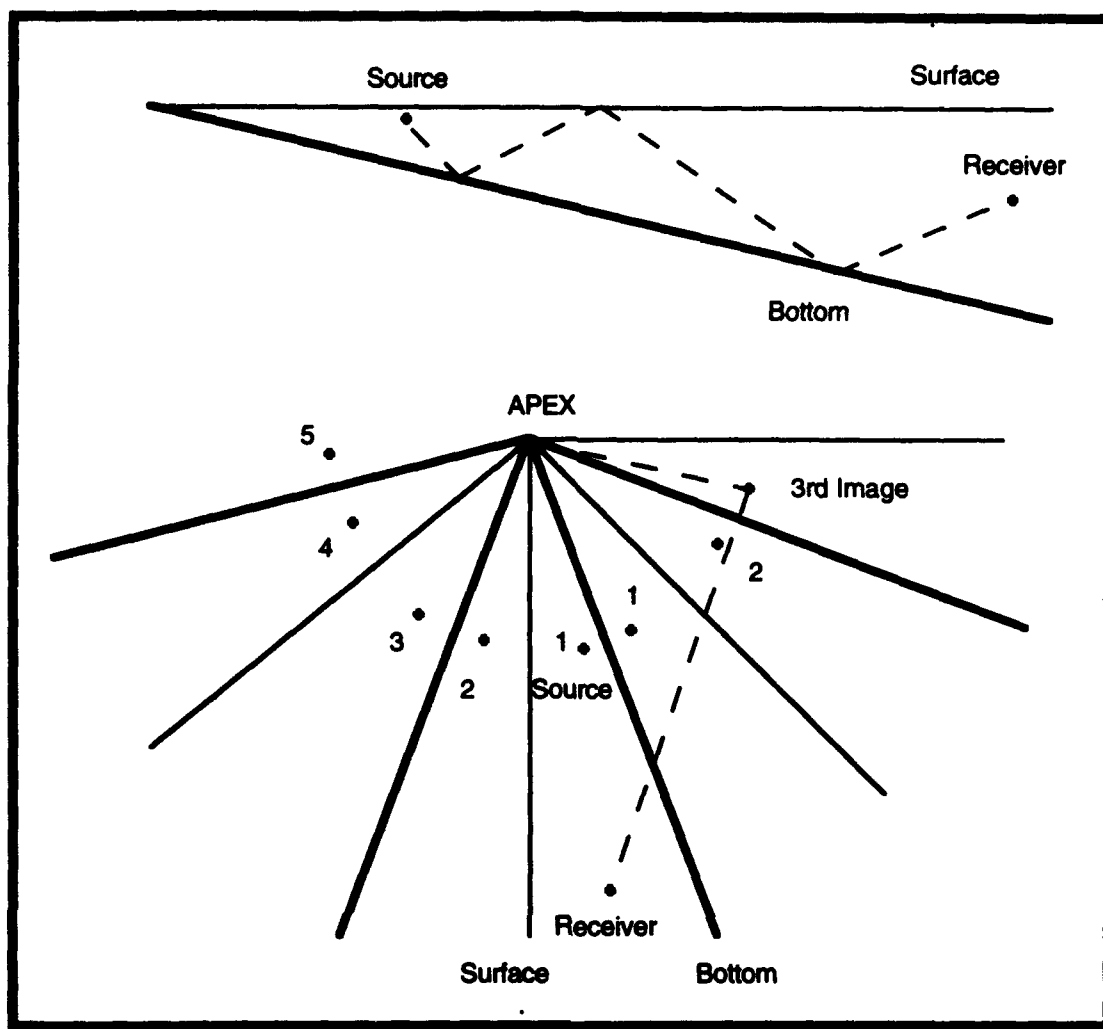


Figure 2-4 - Comparison of Real and Image Theory Sound Propagation Paths

The surface is a pressure release boundary so the incident angle is equal to the reflected angle. The bottom has refractive properties due its composition so the incident angle is not necessarily equal to the transmitted angle but is dependent on the ρ and c ratio of the water and bottom. With each interaction with the bottom, a new angle is produced which is related to the first incident angle. This is discussed later with the reflection coefficient. The lower drawing illustrates the image theory equivalent. The path from the third image to the receiver is a straight line.

The reflection coefficient is a product of the interaction between the boundaries of the fluid layers. The surface is a pressure release boundary so each interaction produces a reflection coefficient of -1. Each interaction with the bottom requires calculation of the reflection coefficient. This coefficient is a function of the speed of sound in each medium, the density of each medium, and the grazing angle of the ray equivalent on the bottom. The sine of the grazing angle θ_{nm} is

$$\sin \theta_{nm+} = \frac{r_1 \sin(\theta_n - 2m\beta) + r_2 \sin[(2m-1)\beta + \delta]}{r_{n+}} \quad (2-6)$$

for the upper images and

$$\sin \theta_{nm-} = \frac{r_1 \sin(\theta_n - 2m\beta) + r_2 \sin[(2m+1)\beta - \delta]}{r_{n-}} \quad (2-7)$$

for the lower images. See (Figure 2-5).

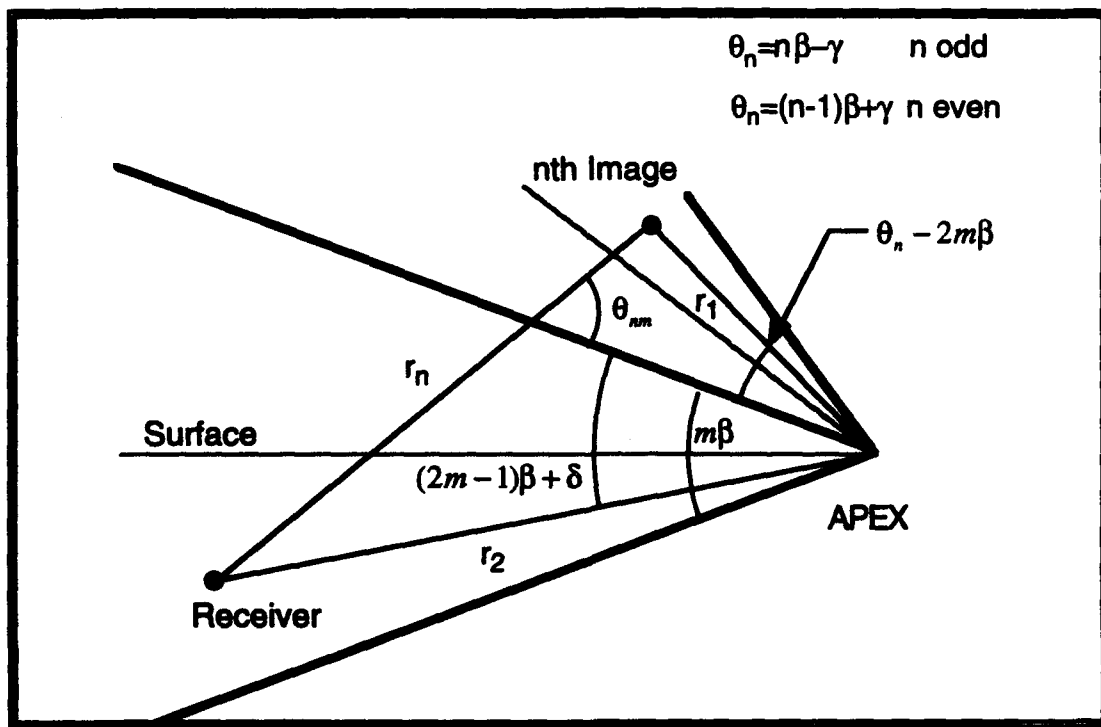


Figure 2-5 - Incident Angle θ_{nm} Calculation (Upper Half Space)

The reflection coefficient for each interaction R_{nm} then is given by

$$R_{nm} = \frac{\frac{\rho_2}{\rho_1} \sin \theta_{nm} - \frac{1}{\sqrt{2}} (\sqrt{b^2 + a^2} + a)^{1/2} + j \frac{1}{\sqrt{2}} (\sqrt{b^2 + a^2} - a)^{1/2}}{\frac{\rho_2}{\rho_1} \sin \theta_{nm} + \frac{1}{\sqrt{2}} (\sqrt{b^2 + a^2} + a)^{1/2} - j \frac{1}{\sqrt{2}} (\sqrt{b^2 + a^2} - a)^{1/2}} \quad (2-8)$$

where ρ_1, ρ_2 are densities of the water and bottom respectively, $j = \sqrt{-1}$, and a and b are given by

$$a = \left(\frac{c_1}{c_2} \right)^2 - \cos^2 \theta_{nm} \quad (2-9)$$

$$b = 2 \left(\frac{c_1}{c_2} \right)^2 \frac{\alpha}{k_2} \quad (2-10)$$

For the above equations, c_1, c_2 are the speeds of sound of the water and bottom, respectively, and α/k_2 is the bottom loss coefficient.

The pressure for each half space is given by summing the contribution for the upper and lower images respectively

$$P_u = \sum_{n=1}^N \frac{1}{r_{n+}} \exp(-jk_1 r_{n+}) (-1)^{INT(n/2)} \prod_{m=1}^M R_{nm+} \quad (2-11)$$

where $\prod R = 1$ when $n=1, 2$ in (2-11) and

$$P_l = \sum_{n=1}^N \frac{1}{r_{n-}} \exp(-jk_1 r_{n-}) (-1)^{INT(n/2)} \prod_{m=0}^M R_{nm-} \quad (2-12)$$

The number of interactions m with the bottom is related to the image number, so the limit M is the integer of $\left[\frac{n+1}{2} \right] - 1$ for the n th image. For convenience we have omitted the factor $e^{j\omega t}$

which would otherwise appear in (2-11) and (2-12).

Two special cases exist in the upper half space. For the case of the direct path of the source to the receiver ($n=1$), R is 1. In the case of a single reflection off the surface and no reflections with the bottom ($n=2$), R is again 1. The phase inversion of the ray is computed by the $(-1)^{INT(n/2)}$ term of (2-11) and (2-12).

Since the model is frequency independent, a scaling distance X_c is used. X_c is defined as the distance where the lowest normal mode attains cutoff when the bottom is fast ($c_2 > c_1$).

This cutoff distance is calculated by

$$k_1 X_c = \frac{\pi}{2 \sin \theta_c \tan \beta} \quad \theta_c = \cos^{-1} \left(\frac{c_1}{c_2} \right) \quad (2-13)$$

so,

$$X_c = \frac{\pi}{2 k_1 \sin \theta_c \tan \beta} \quad (2-14)$$

For a slow bottom an analogous scaling, convenient for the computer program is

$$k_1 X_c = \frac{\pi}{2 \tan \theta_s \tan \beta} \quad \theta_s = \cos^{-1} \left(\frac{c_2}{c_1} \right) \quad (2-15)$$

so,

$$X_c = \frac{\pi}{2 k_1 \tan \theta_s \tan \beta} \quad (2-16)$$

For the total pressure at the receiver, the upper and lower contributions are combined, thus

$$P = P_u + P_l \quad (2-17)$$

III. DOUBLET FORMATION

A. GENERAL DESCRIPTION

An acoustic doublet is a pair of acoustic images 180° out of phase. The first doublet consists of the source and its reflection, the 2nd upper image. This is called a neutral doublet ($n=0$). The reflection coefficient is 1 because its midpoint does not encounter a

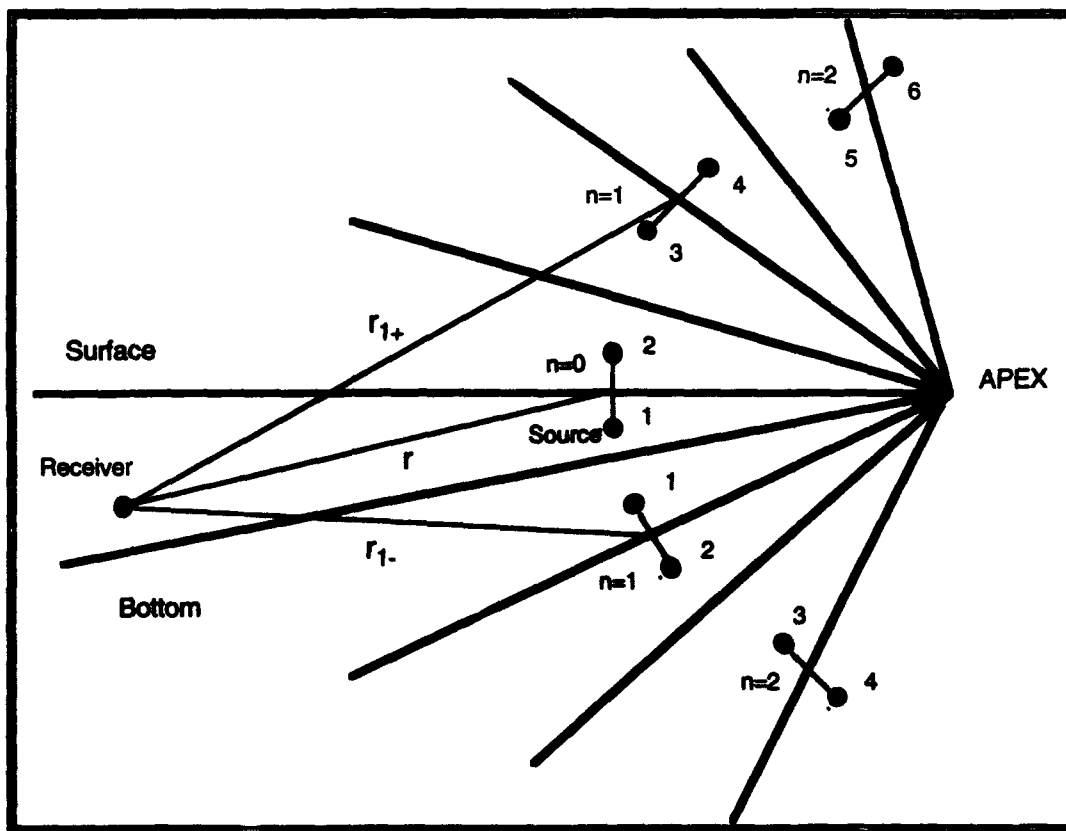


Figure 3-1 - Doublet Image Structure

boundary. The 3rd and 4th upper images are the 1st upper doublet ($n=1$). The 5th and 6th upper images are the 2nd upper doublet ($n=2$). The 1st and 2nd lower images are the 1st

lower doublet ($n=1$) and the 3rd and 4th lower images are the 2nd lower doublet ($n=2$).

This procedure is continued until the opposite surface is reached. See Figure 3-1.

The total number of acoustic doublet pairs is given by

$$N = \text{Int} \left(\frac{\text{Int} \left(\frac{360^\circ}{\beta} \right) - 2}{4} \right) \quad (3-1)$$

At worst, only three images will be missed and they will be in the higher order images of the source so their contribution is negligible due to all the reflection coefficients encountered [Ref. 25].

B. DEVELOPMENT

The sound propagation for a spherically spreading point source is

$$P = \frac{A}{r} e^{j(\omega t - kr)} \quad (3-2)$$

where A is the pressure amplitude, r is the range from the source and k is the wave number ω/c [Ref. 11]. When two sources are combined to form a doublet, the above equation can be expanded to

$$P = \frac{A_+}{r_-} e^{j(\omega t - kr_-)} - \frac{A_-}{r_+} e^{j(\omega t - kr_+)} \quad (3-3)$$

where the subscripts "+" and "-" refer to the upper and lower sources of the doublet and

$$\begin{aligned} r_+ &= r + \Delta r & A_+ &= A + \Delta A \\ r_- &= r - \Delta r & A_- &= A - \Delta A \end{aligned} \quad (3-4)$$

The delta values are the incremental difference between each source compared to the theoretical point source. Figure 3-2 illustrates the doublet close-up. The distance d is the

separation of the images of the doublet pair and r is the distance of the doublet midpoint to the receiver.

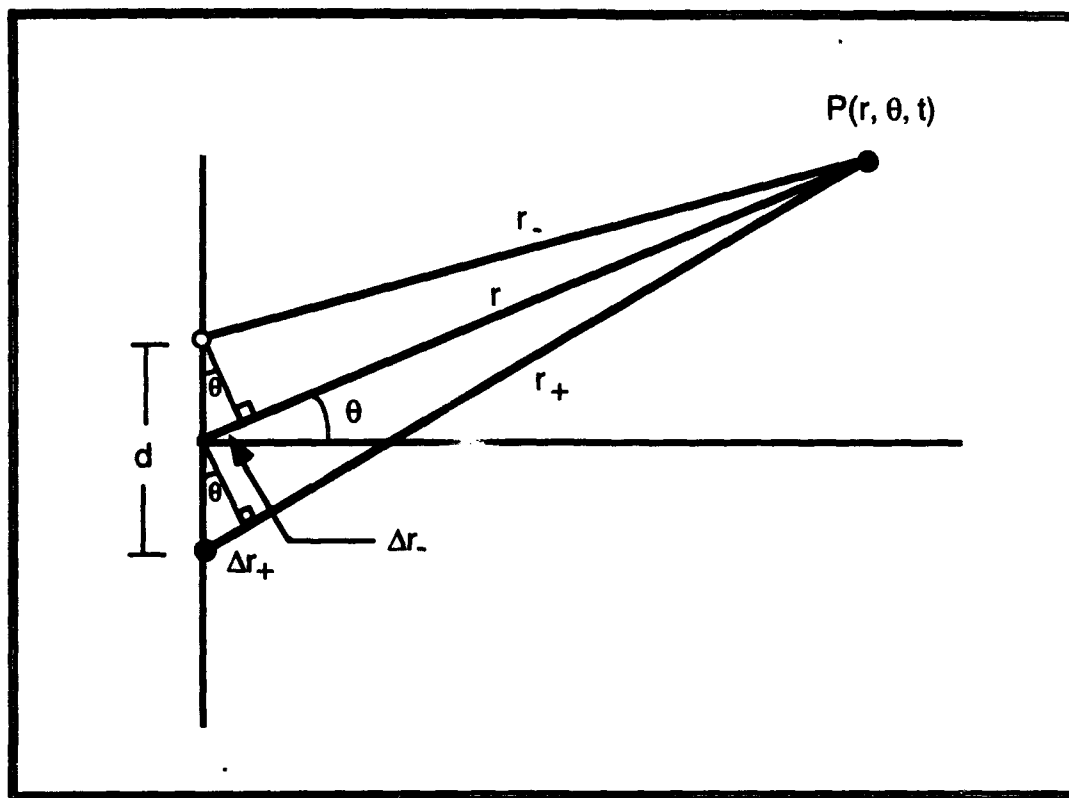


Figure 3-2 - Doublet Close-Up

The pressure equation can now be rewritten as

$$P = \frac{A}{r} e^{j(\omega t - kr)} \left[\left(\frac{A + \Delta A}{r - \Delta r} \right) e^{jk\Delta r_-} \left(\frac{A - \Delta A}{r + \Delta r} \right) e^{-jk\Delta r_+} \right] \quad (3-5)$$

1. Balanced Doublet

The 1st upper image has an reflection image of equal amplitude and opposite phase which is the second upper image. In the far field, the image pair is treated as a single doublet source. See Figure 3-3.

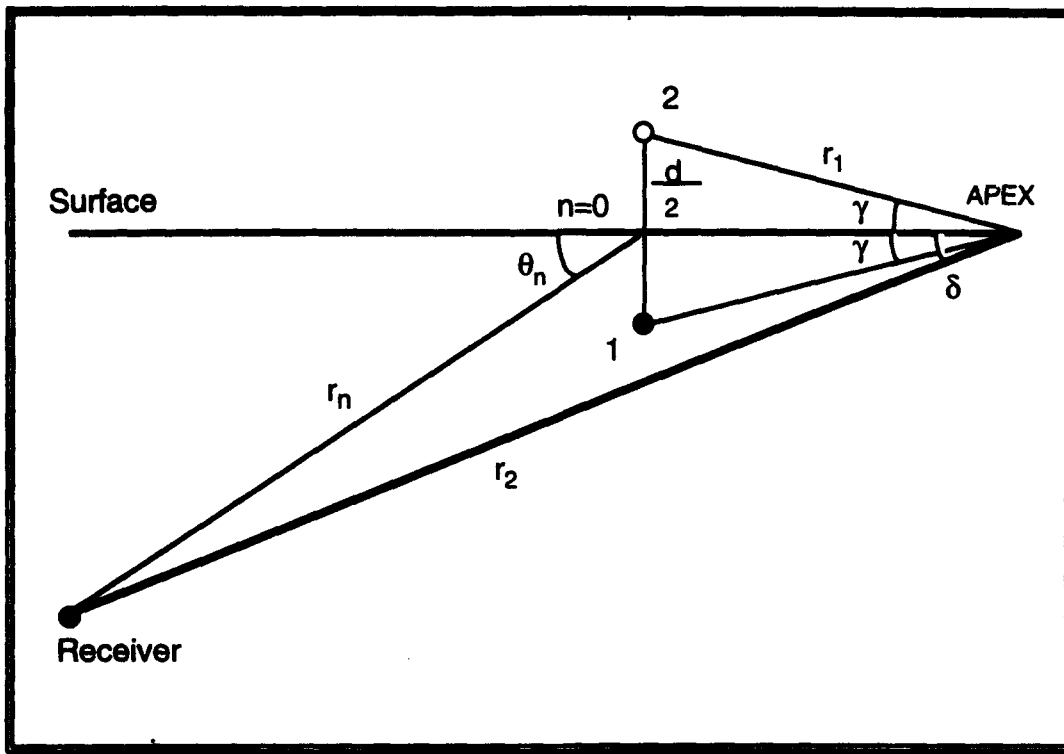


Figure 3-3 - Geometry of Neutral Doublet

The pressure equation for a balanced source can be approximated by

$$P = \frac{A}{r} e^{j\omega t} \left[e^{-jk(r-\Delta r)} - e^{-jk(r+\Delta r)} \right] \quad (3-6)$$

The geometry of the doublet is given in Figure 3-2. Δr is

$$\Delta r = \frac{d}{2} \sin(\theta) = r_1 \sin(\gamma) \sin(\theta) \quad (3-7)$$

By substituting Equation 3-7 into Equation 3-6 and factoring one gets

$$P = \frac{A}{r} e^{j\omega t} \left[e^{-jkr} \left(e^{jkr_1 \sin(\gamma) \sin(\theta)} - e^{-jkr_1 \sin(\gamma) \sin(\theta)} \right) \right] \quad (3-8)$$

By using the relationship of

$$\sin(x) = \frac{e^{jx} - e^{-jx}}{2j} \quad (3-9)$$

where $x = kr_1 \sin(\gamma) \sin(\theta)$, the result is

$$P = 2j \frac{A}{r} \sin(kr_1 \sin(\gamma) \sin(\theta)) e^{j(ax - kr)} \quad (3-10)$$

2. Unbalanced Doublet

For the unbalanced doublet, the amplitude relationship is expressed as

$$A_o = \frac{A_+ + A_-}{2} \quad \Delta A = \frac{A_+ - A_-}{2} \quad (3-11)$$

The unbalanced doublet can be viewed as a combination of a balanced doublet on which is superimposed a like-charge doublet [Ref. 28]. See Figure 3-4

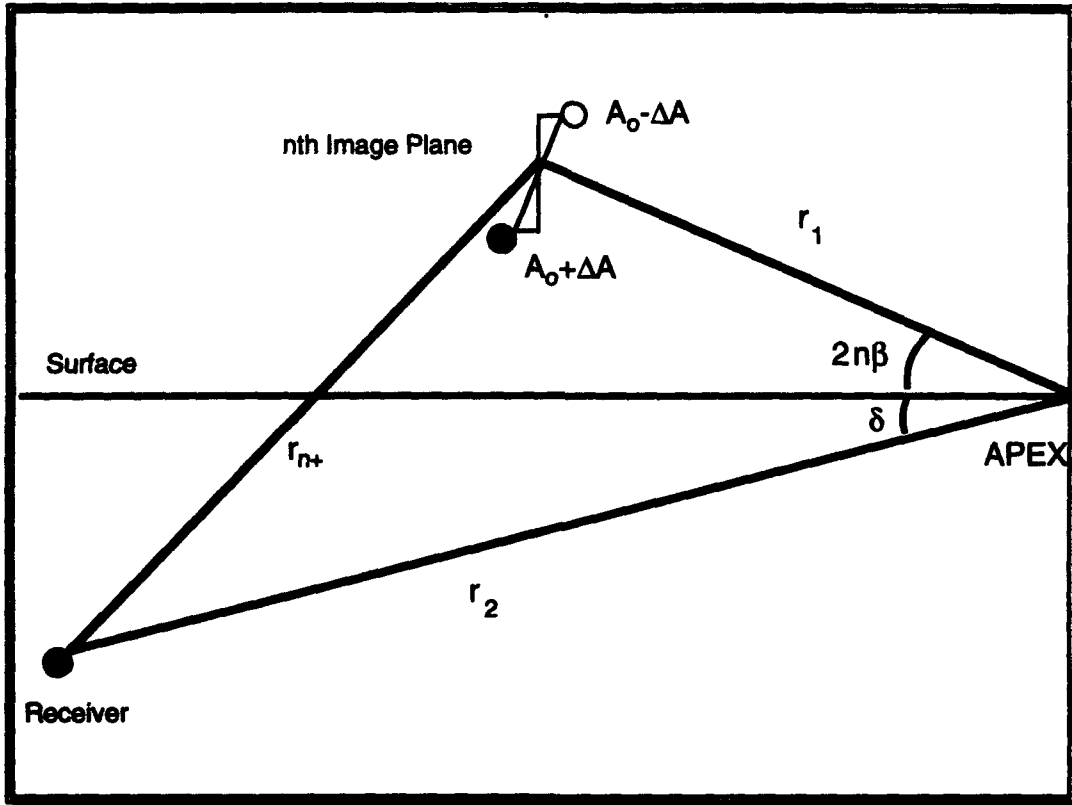


Figure 3-4 - Geometry of Unbalanced Doublet

The pressure equation is

$$P = \left[2j \frac{A_o}{r} \sin(kr_1 \sin(\gamma) \sin(\theta)) + 2 \frac{\Delta A}{r} \cos(kr_1 \sin(\gamma) \sin(\theta)) \right] e^{j(ax - kr)} \quad (3-12)$$

which can be rewritten as

$$P = 2j \frac{A_o}{r} \left[\sin(kr_1 \sin(\gamma) \sin(\theta)) - j \frac{\Delta A}{A_o} \cos(kr_1 \sin(\gamma) \sin(\theta)) \right] e^{j(ax - kr)} \quad (3-13)$$

3. Distance from Doublet to Receiver

The distance from the doublet formation to the receiver can be calculated using the law of cosines. For a three dimensional wedge, the following equation is used

$$r_{n\pm}^2 = r_1^2 + r_2^2 + y_0^2 - 2r_1r_2 \cos(2n\beta \pm \delta) \quad (3-14)$$

where r_1 and r_2 are the ranges from the apex to source and receiver respectively, y_0 is the cross-slope range, β is the wedge angle, δ is the source angle, and n is the doublet formation number. The "+" and "-" signs are reference to the upper or lower images in the doublet formation. See Figure 3-5.

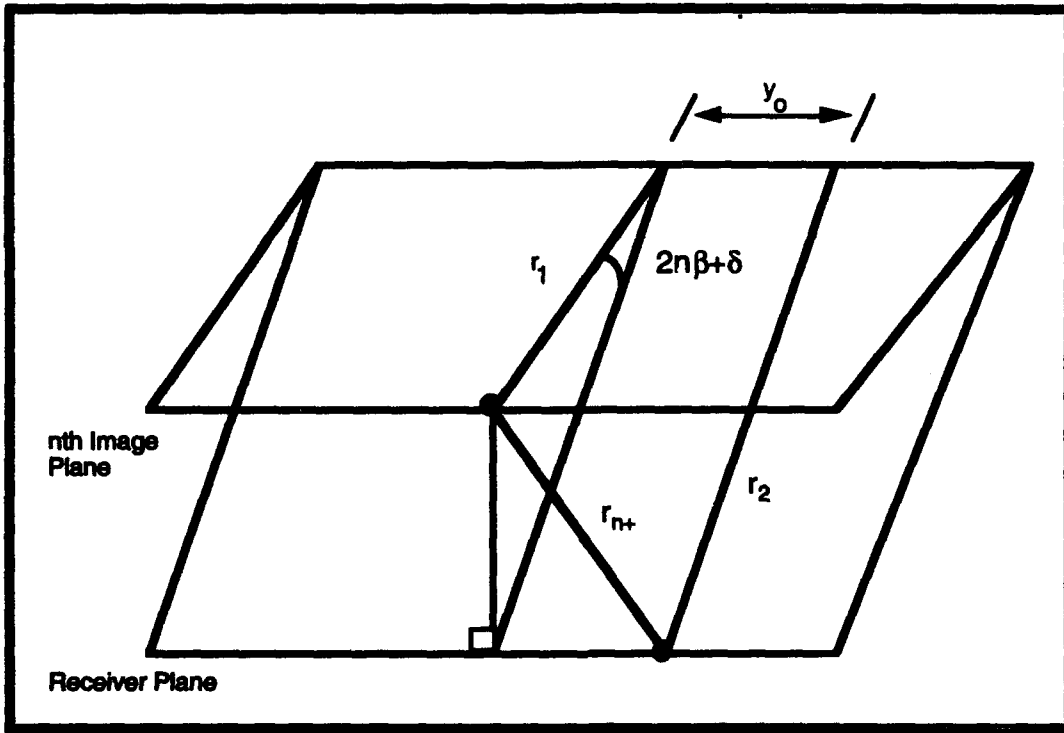


Figure 3-5 - Doublet Three Dimensional Geometry

Equation 3-13 can be rewritten by adding and subtracting $2r_1r_2$. This yields the following expression

$$r_{n\pm}^2 = r_1^2 - 2r_1r_2 + r_2^2 + y_0^2 + 2r_1r_2 - 2r_1r_2 \cos(2n\beta \pm \delta) \quad (3-15)$$

By combining terms and factoring, the following is the result

$$r_{n\pm}^2 = (r_1 - r_2)^2 \left[1 + \frac{y_0^2}{(r_1 - r_2)^2} + \frac{2r_1r_2}{(r_1 - r_2)^2} (1 - \cos(2n\beta \pm \delta)) \right] \quad (3-16)$$

or

$$r_{n\pm} = |r_1 - r_2| \sqrt{1 + \frac{y_0^2}{(r_1 - r_2)^2} + \frac{2r_1r_2}{(r_1 - r_2)^2} (1 - \cos(2n\beta \pm \delta))} \quad (3-17)$$

4. Pressure From Each Doublet

A generalization of Equation 3-13 can be made by substituting A_n and ΔA_n for A_o and ΔA where

$$A_n = \frac{A_{n+} + A_{n-}}{2} \quad \Delta A_n = \frac{A_{n+} - A_{n-}}{2} \quad (3-18)$$

and θ_n for θ where

$$\theta_{n\pm} = 2n\beta \pm \delta \quad (3-19)$$

so the pressure from each doublet is

$$P_{n\pm} = 2j \frac{A_{n\pm}}{r_{n\pm}} \left[\sin(kr_1 \sin(\gamma) \sin(\theta_{n\pm})) - j \frac{\Delta A_{n\pm}}{A_{n\pm}} \cos(kr_1 \gamma \sin(\theta_{n\pm})) \right] e^{j(\omega t - kr)} \quad (3-20)$$

IV. QUADRUPLLET FORMATION

A. QUADRUPLLET GENERAL DESCRIPTION

A quadruplet is formed by combining the upper and lower doublets. The visualization

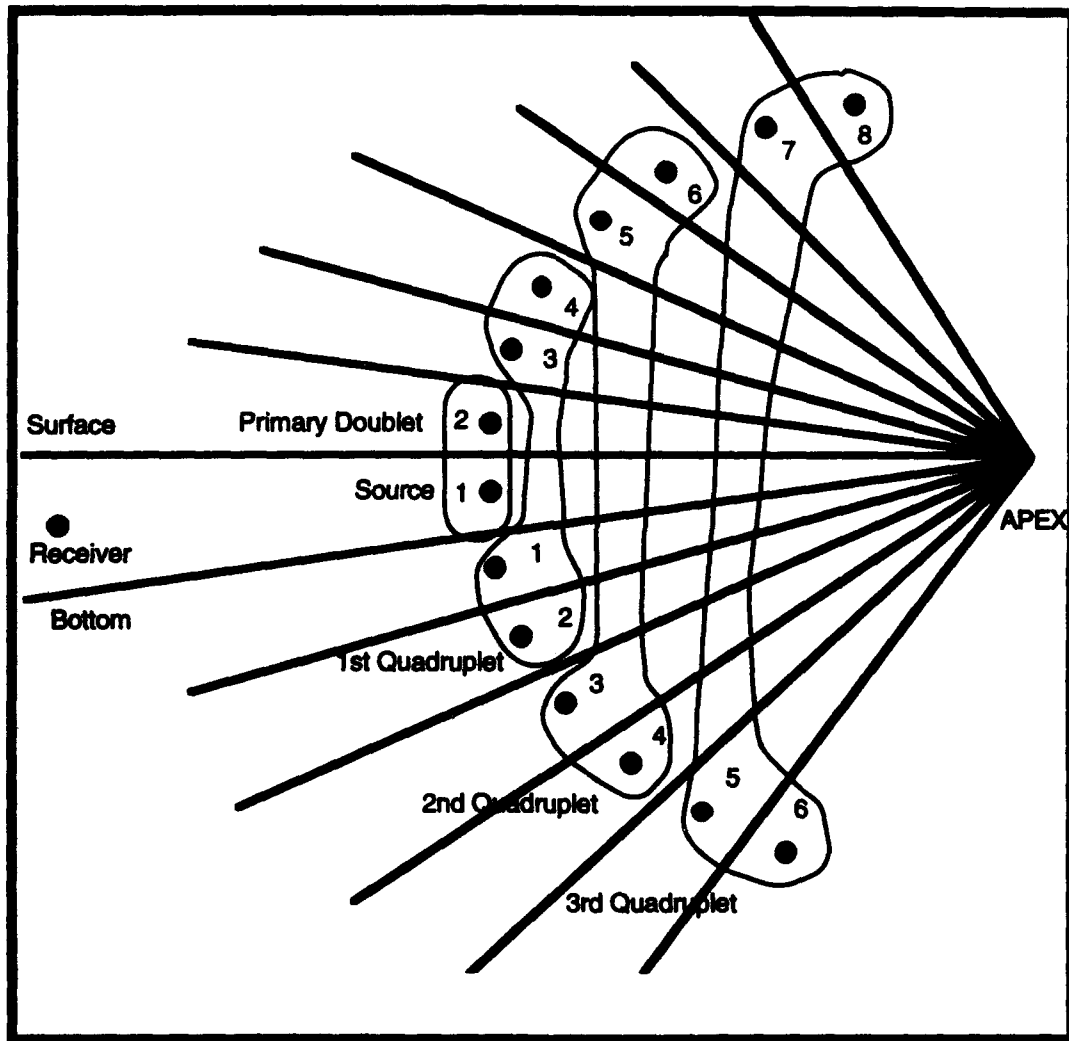


Figure 4-1 - Quadruplet Illustration

of the quadruplet is illustrated in Figure 4-1. The primary doublet (the source and its first upper image) are considered separately. The first quadruplet consists of the third and

fourth upper image (first upper doublet) and the first and second lower image (first lower doublet). The second quadruplet consists of the fifth and sixth upper images (second upper doublet) and the third and fourth lower images (second lower doublet). The process is continued until the opposite surface is reached.

The number of quadruplets formed is

$$N = \text{Int}\left(\frac{90}{\beta}\right) \quad (4-1)$$

At worst, only 3 images will be missed and they are highest order images so their contribution is negligible due to all the reflection coefficients encountered.

B. QUADRUPLER DEVELOPMENT

1. Balanced Quadruplet

The complementary doublets are 180° out of phase. The pressure of the quadruplet is given by combining the nth upper and lower doublets from Equation. 3-10 of the balanced doublet to form

$$P_n = 2j \frac{A_n}{r_n} \left[\sin(kr_1 \sin(\gamma) \sin(\theta_{n+})) e^{-jk\Delta r_{n+}} - \sin(kr_1 \sin(\gamma) \sin(\theta_{n-})) e^{-jk\Delta r_{n-}} \right] e^{j(\omega - kr)} \quad (4-2)$$

By substituting Equation 3-19 for $\theta_{n\pm}$ and using the approximation that $\sin(\gamma) = \gamma$, the balanced quadruplet pressure equation is

$$P_n = 2j \frac{A_n}{r_n} \left[\sin(kr_1 \gamma \sin(2n\beta + \delta)) e^{-jk\Delta r_{n+}} - \sin(kr_1 \gamma \sin(2n\beta - \delta)) e^{-jk\Delta r_{n-}} \right] e^{j(\omega - kr)} \quad (4-3)$$

2. Unbalanced Quadruplet

The amplitudes of the upper and lower doublets are not equal because of the distance differential between them as seen in Figure 4-2. This leads to the concept of the unbalanced quadruplet.

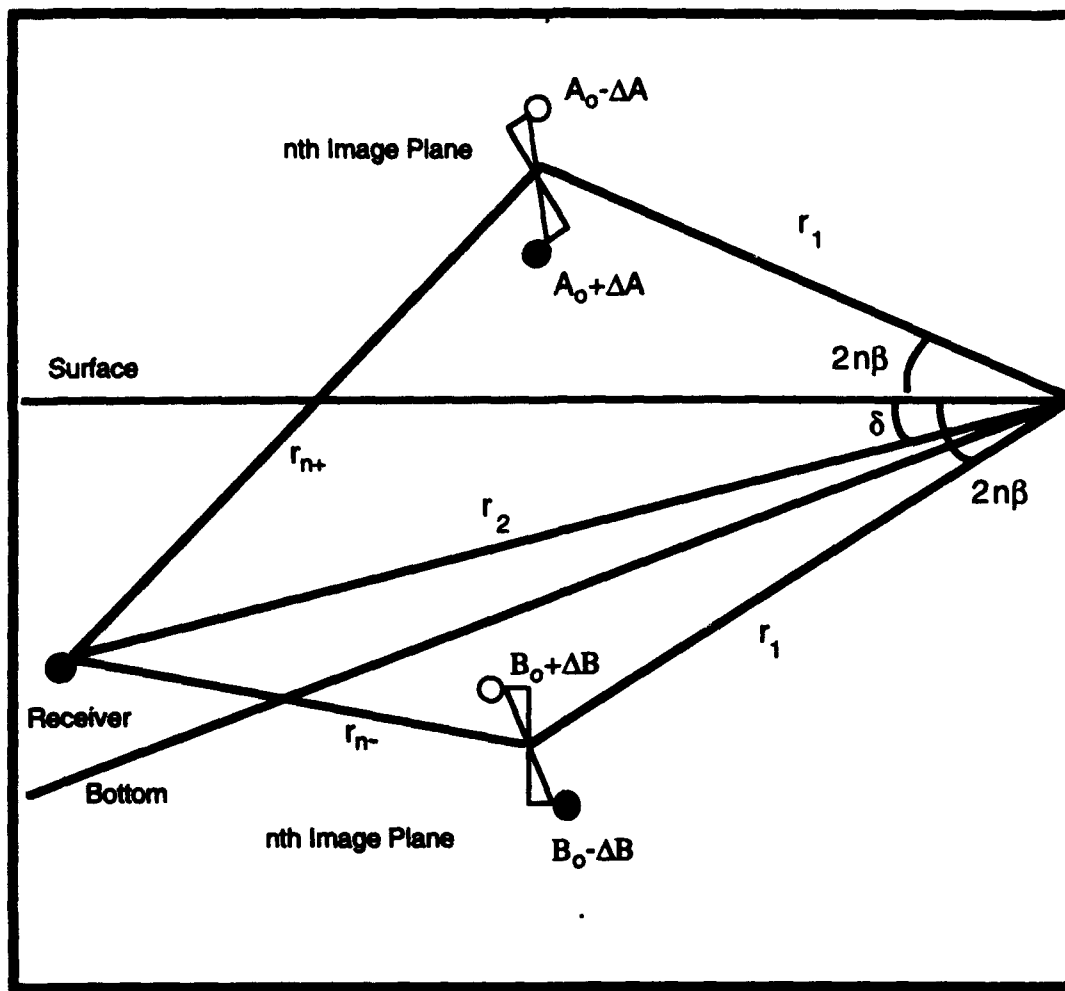


Figure 4-2 - Illustration of Unbalanced Quadruplet Amplitude

The Δr terms are derived from the comparison of the distance from the primary doublet to the midpoint of the upper and lower doublets in each quadruplet (Figure 4-2). This ensures that all phase angles are calculated from a common reference point. Using Equation 3-17, by setting $y_0=0$, we can make the following approximation,

$$r_{n\pm} = |r_1 - r_2| \sqrt{1 + \frac{2r_1 r_2}{(r_1 - r_2)^2} (1 - \cos(2n\beta \pm \delta))} \quad (4-4)$$

$$r_{n\pm} \equiv |r_1 - r_2| \left[1 + \frac{r_1 r_2}{(r_1 - r_2)^2} (1 - \cos(2n\beta \pm \delta)) \right] \quad (4-5)$$

Now Δr_n can be approximated using the following relation

$$\Delta r_{n\pm} = r_{n\pm} - |r_1 - r_2| \equiv \frac{r_1 r_2}{|r_1 - r_2|} [1 - \cos(2n\beta \pm \delta)] \quad (4-6)$$

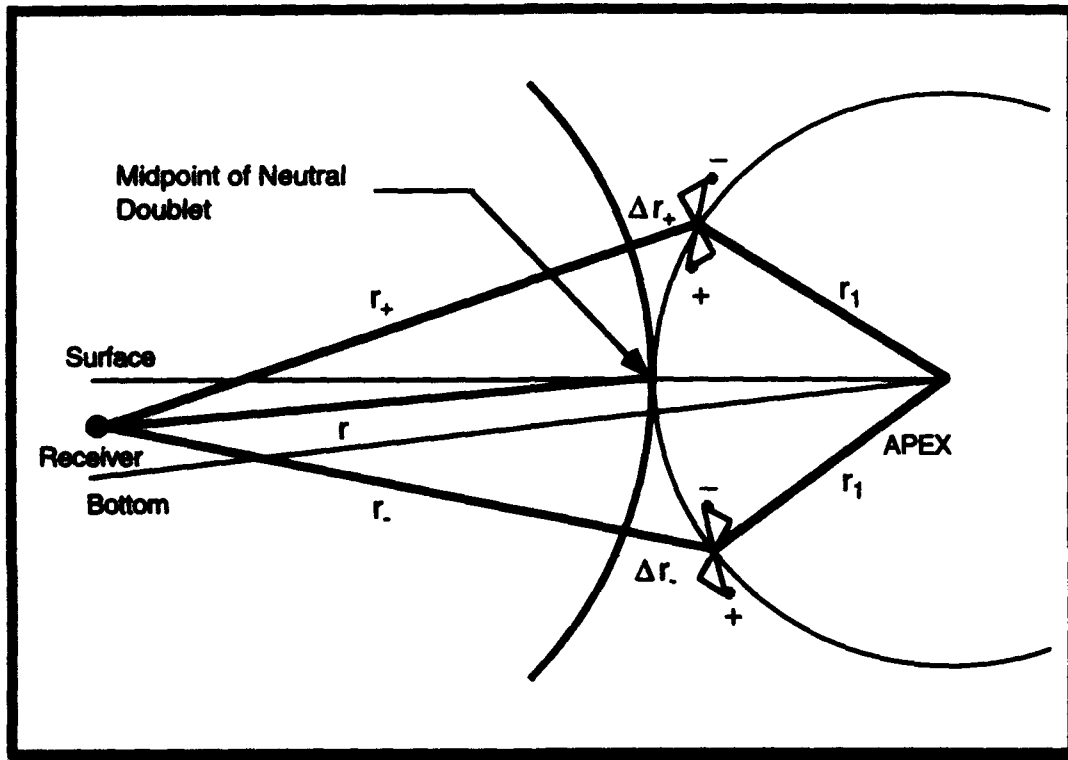


Figure 4-3 - Illustration of Δr in a Quadruplet

The cosine term in the above expression can be expanded using a trigonometric identity

$$\cos(2n\beta \pm \delta) = \cos(2n\beta)\cos(\delta) \pm \sin(\delta)\sin(2n\beta) \quad (4-7)$$

Small angle approximations can be used for δ where $\cos(\delta) \approx 1$ and $\sin(\delta) \approx \delta$ so

$$\cos(2n\beta \pm \delta) \approx \cos(2n\beta) \pm \delta \sin(2n\beta) \quad (4-8)$$

Equation 4-8 can be substituted into Equation 4-6 which can be substituted into Equation 4-3 to yield

$$P_n = \frac{2jA_n}{r} e^{j(\omega t - kr)} e^{-jk\left(\frac{r_1 r_2}{r_2 - r_1}\right)(1 - \cos(2n\beta))} \left[\sin(kr_1 \gamma \sin(2n\beta + \delta)) e^{-jk\left(\frac{r_1 r_2}{r_2 - r_1}\right)\delta \sin(2n\beta)} \right. \\ \left. - \sin(kr_1 \gamma \sin(2n\beta - \delta)) e^{jk\left(\frac{r_1 r_2}{r_2 - r_1}\right)\delta \sin(2n\beta)} \right] \quad (4-9)$$

For convenience, the following terms are defined

$$\begin{aligned} \phi &= kr_1 \mu (1 - \cos(2n\beta)) \\ d &= kr_1 \delta \sin(2n\beta) \\ \mu &= \frac{r_2}{|r_1 - r_2|} \end{aligned} \quad (4-10)$$

Equation 4-9 now becomes

$$P_n = \frac{2jA_n}{r} e^{j(\omega t - kr)} e^{-j\phi} \left[\sin(kr_1 \gamma \sin(2n\beta + \delta)) e^{-j\mu d} \right. \\ \left. - \sin(kr_1 \gamma \sin(2n\beta - \delta)) e^{j\mu d} \right] \quad (4-11)$$

The amplitudes of the upper and lower images of the doublets are not equal. By separating the amplitudes and distributing it into the main equation in a process similarly done in Equation 3-12 and 3-13, the unbalanced quadruplet equation is the result

$$P_n = \frac{2j}{r} e^{j(\omega t - kr)} e^{-j\phi} \left[A_n \left[\sin(kr_1 \gamma \sin(2n\beta + \delta)) - j \frac{\Delta A_n}{A_n} \cos(kr_1 \gamma \sin(2n\beta + \delta)) \right] e^{-j\mu d} \right. \\ \left. - B_n \left[\sin(kr_1 \gamma \sin(2n\beta - \delta)) - j \frac{\Delta B_n}{B_n} \cos(kr_1 \gamma \sin(2n\beta - \delta)) \right] e^{j\mu d} \right] \quad (4-12)$$

where A_n and B_n are the amplitudes of the upper and lower n th doublets at the midpoint and ΔA_n and ΔB_n are the differences in amplitude of the n th upper and lower doublet images.

V. REFLECTION COEFFICIENTS

A. REFLECTION COEFFICIENTS

The reflection coefficient is discussed in Chapter 2 with the image theory development. The reflection coefficient from [Ref. 29] is

$$R_{nm} = \frac{\frac{\rho_2}{\rho_1} \sin(\theta_{nm}) - \frac{c_1}{c_2} \sin(\theta_i)}{\frac{\rho_2}{\rho_1} \sin(\theta_{nm}) + \frac{c_1}{c_2} \sin(\theta_i)} \quad (5-1)$$

It can be rewritten as

$$R_{nm} = \frac{bc - \frac{\sin(\theta_i)}{\sin(\theta_{nm})}}{bc + \frac{\sin(\theta_i)}{\sin(\theta_{nm})}} \quad (5-2)$$

where θ_{nm} is the grazing angle of the nth image going through the mth plane and

$$b = \frac{\rho_2}{\rho_1} \quad c = \frac{c_2}{c_1} \quad (5-3)$$

$\sin(\theta_c)$ can be expanded and the reflection coefficient can be rewritten as

$$R_{nm} = \frac{bc - \frac{\sqrt{1 - c^2 \cos^2(\theta_{nm})}}{\sin(\theta_{nm})}}{bc + \frac{\sqrt{1 - c^2 \cos^2(\theta_{nm})}}{\sin(\theta_{nm})}} \quad (5-4)$$

The term under the radical can be manipulated and written in terms of the critical angle, θ_c , from Equation 2-13

$$\sqrt{1 - c^2 \cos^2(\theta_{nm})} = \sqrt{1 - \frac{\cos^2(\theta_{nm})}{\cos^2(\theta_c)}} = c \sqrt{\sin^2(\theta_{nm}) - \sin^2(\theta_c)} \quad (5-5)$$

Equation 5-5 can be combined into Equation 5-4 and simplified.

$$R_{nm} = \frac{b - \sqrt{1 - \left(\frac{\sin(\theta_c)}{\sin(\theta_{nm})} \right)^2}}{b + \sqrt{1 - \left(\frac{\sin(\theta_c)}{\sin(\theta_{nm})} \right)^2}} \quad (5-6)$$

By using the substitution

$$x = \frac{\sin(\theta_{nm})}{\sin(\theta_c)} \quad (5-7)$$

the reflection coefficient takes the form

$$R_{nm} = \frac{b - \sqrt{1 - \frac{1}{x^2}}}{b + \sqrt{1 - \frac{1}{x^2}}} \quad (5-8)$$

B. SLOW BOTTOM REFLECTION COEFFICIENTS

A slow bottom is when the speed of sound in the bottom material is slower than in the water ($c_1 > c_2$). This is an easier case to handle because there is no critical angle constraint, the reflection coefficient is real and diminishes quickly to zero.

Equation 5-8 can be expanded to by using

$$\sin(\theta_c) = 1 - \frac{1}{c^2} = \frac{c^2 - 1}{c^2} \quad (5-9)$$

resulting in

$$R_{nm} = \frac{b - \sqrt{1 - \left(\frac{c^2 - 1}{c^2}\right) \frac{1}{\sin^2(\theta_{nm})}}}{b + \sqrt{1 - \left(\frac{c^2 - 1}{c^2}\right) \frac{1}{\sin^2(\theta_{nm})}}} \quad (5-10)$$

Reversing the order of the terms

$$R_{nm} = \frac{b - \sqrt{\left(\frac{1 - c^2}{c^2}\right) \frac{1}{\sin^2(\theta_{nm})} + 1}}{b + \sqrt{\left(\frac{1 - c^2}{c^2}\right) \frac{1}{\sin^2(\theta_{nm})} + 1}} \quad (5-11)$$

By pulling out the first term

$$R_{nm} = \frac{b - \sqrt{\frac{1 - c^2}{c^2} \frac{1}{\sin(\theta_{nm})}} \sqrt{1 + \frac{c^2}{1 - c^2} \sin(\theta_{nm})}}{b + \sqrt{\frac{1 - c^2}{c^2} \frac{1}{\sin(\theta_{nm})}} \sqrt{1 + \frac{c^2}{1 - c^2} \sin(\theta_{nm})}} \quad (5-12)$$

Dividing the top and bottom by $1/b$ and making an approximation with the square root results in

$$R_{nm} \cong \frac{1 - \sqrt{\frac{1 - c^2}{c^2} \frac{1}{b \sin(\theta_{nm})}} \left(1 + \frac{1}{2} \frac{c^2}{1 - c^2} \sin^2(\theta_{nm})\right)}{1 + \sqrt{\frac{1 - c^2}{c^2} \frac{1}{b \sin(\theta_{nm})}} \left(1 + \frac{1}{2} \frac{c^2}{1 - c^2} \sin^2(\theta_{nm})\right)} \quad (5-13)$$

Using the relation of

$$\frac{1 - \psi}{1 + \psi} \cong e^{-2\psi} \quad (5-14)$$

Equation 5-13 can be approximated by

$$R_{nm} \cong e^{-\frac{2bc}{\sqrt{1 - c^2}} \theta_{nm}} \quad (5-15)$$

Substituting

$$\alpha = \frac{2bc}{\sqrt{1-c^2}} \quad (5-16)$$

The final product is

$$R_{nm} \equiv e^{-\alpha\theta_{nm}} \quad (5-17)$$

Each ray intersects the bottom $2n-1$ times. The product of the reflection coefficients will be

$$R_n = \prod R[\theta_m] \quad (5-18)$$

Expanding the equation yields

$$R_n = \prod_{m=1,3,\dots}^{2n-1} R[\theta_m] = e^{-\alpha(\eta+\beta)} e^{-\alpha(\eta+3\beta)} e^{-\alpha(\eta+5\beta)} \dots e^{-\alpha(\eta+(2n-1)\beta)} \quad (5-19)$$

where $\eta = \varepsilon + \delta$. Multiplying exponentials with the same base is equivalent to add their exponents. The terms in can be rearranged to

$$\prod_{m=1,3,\dots}^{2n-1} R[\theta_m] = e^{-n\alpha\eta} e^{-\alpha[1+3+5\dots(2n-1)]\beta} \quad (5-20)$$

By noticing that the sum of the exponentials at a index is equal to the index squared, the result is

$$R_n = e^{-n\alpha\eta} e^{-n^2\alpha\beta} \quad (5-21)$$

For small angles, the first term in the exponential is very small compared to the second so the cumulative reflection coefficient for a slow bottom is

$$R_n = e^{-n^2\alpha\beta} \quad (5-22)$$

C. FAST BOTTOM REFLECTION COEFFICIENTS

A fast bottom is when the speed of sound in the bottom is faster than the speed of sound of water ($c_2 > c_1$). At angles below grazing, the acoustic energy will propagate with

100% reflectance ($R_{nm}=1$) until θ_c (see Equation 2-13) is reached then will decay. See Figure 5-1.

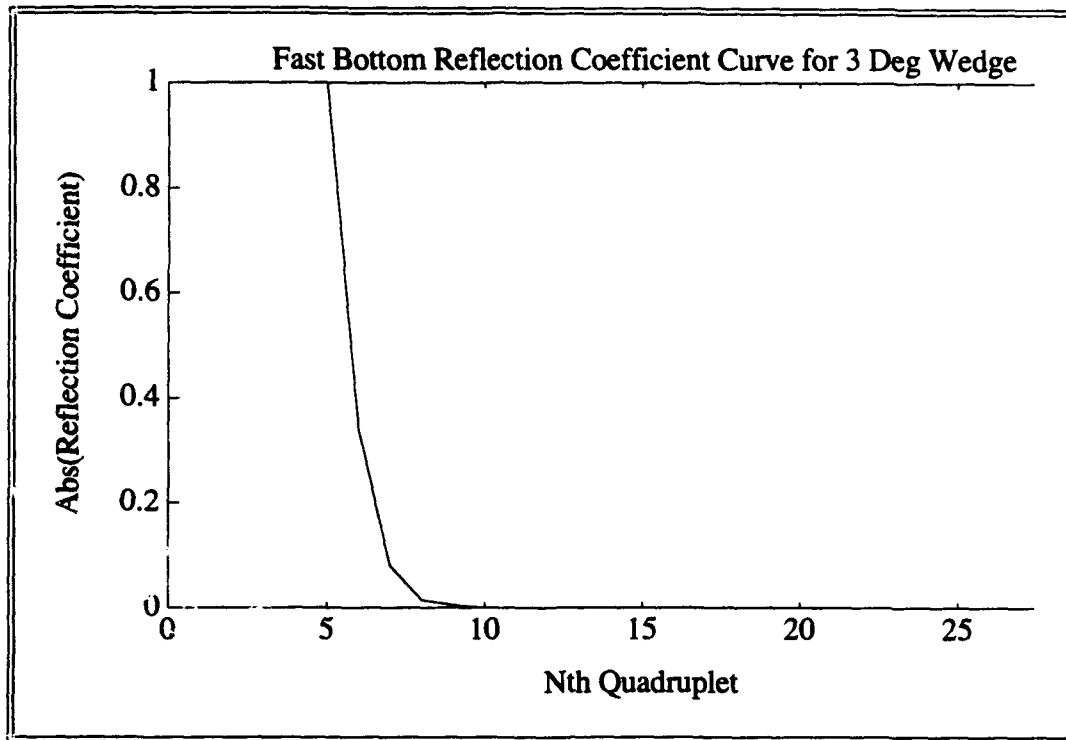


Figure 5-1 - Typical Fast Bottom Cumulative Reflection Coefficient Curve

The development follows until Equation 5-8. By reversing the order of terms

$$R_{nm} = \frac{b + j\sqrt{\frac{1}{x^2} - 1}}{b - j\sqrt{\frac{1}{x^2} - 1}} \quad (5-23)$$

The above equation can be simplified to

$$R_{nm} = \frac{1 + \frac{j}{b}\sqrt{\frac{1}{x^2} - 1}}{1 - \frac{j}{b}\sqrt{\frac{1}{x^2} - 1}} \quad (5-24)$$

Using the Maclaurin series [Ref. 30] of

$$\ln \frac{1+z}{1-z} = 2 \tanh^{-1}(z) \quad (5-25)$$

Equation 5-22 results in

$$R_{nm} = e^{2 \tanh^{-1} \left(\frac{j}{b} \sqrt{\frac{1}{x^2} - 1} \right)} \quad (5-26)$$

By taking out the $1/x^2$ term and inverting the \tanh^{-1}

$$R_{nm} = e^{\left(\pi - 2 \tanh^{-1} \left(j \frac{bx}{\sqrt{1-x^2}} \right) \right)} \quad (5-27)$$

Simplifying the above equation results in

$$R_{nm} = -e^{-2 \tanh^{-1} \left(j \frac{bx}{\sqrt{1-x^2}} \right)} \quad (5-28)$$

or

$$R_{nm} = -e^{-2j \tan^{-1} \left(\frac{bx}{\sqrt{1-x^2}} \right)} \quad (5-29)$$

The cumulative reflection coefficient is the cumulative product of all previous reflection coefficients and will take the form of

$$R_n = \prod_{n=1}^N R_{nm} = \prod_{n=1}^N -e^{-2j \tan^{-1} \left(\frac{bx}{\sqrt{1-x^2}} \right)} \quad (5-30)$$

VI. GRAZING AND RECEIVER ANGLES IN QUADRUPLLET

A. RECEIVER ANGLE

The receiver angle is calculated using the law of sines. The relation can be seen in Figure 6-1

$$\frac{r_1}{\sin(\epsilon_{n\pm})} = \frac{r_{n\pm}}{\sin(2n\beta \pm \delta)} \quad (6-1)$$

By solving for $\sin(\epsilon_n)$ and using the small angle approximation

$$\epsilon_{n\pm} = \frac{r_1}{r_{n\pm}} \sin(2n\beta \pm \delta) \quad (6-2)$$

Likewise the receiver angle for each image of the doublets can be solved for. The receiver angle for the upper half-space is given by

$$\frac{r_1}{\sin(\epsilon_{n+\pm})} = \frac{r_{n+\pm}}{\sin(2n\beta + \delta \pm \gamma)} \quad (6-3)$$

$$\sin(\epsilon_{n+\pm}) = \frac{r_1}{r_{n+\pm}} \sin(2n\beta + \delta \pm \gamma) \quad (6-4)$$

Using a the sine expansion of the sum of two angles, the above equation results in

$$\sin(\epsilon_{n+\pm}) = \frac{r_1}{r_{n\pm}} [\sin(2n\beta + \delta) \cos(\gamma) \pm \cos(2n\beta + \delta) \sin(\gamma)] \quad (6-5)$$

Making the assumption $\cos(\gamma)=1$, $\sin(\gamma)=\gamma$, $\sin(\epsilon)=\epsilon$, $r_{n+\pm} = r_{n\pm}$ and substituting $\sin(\epsilon_n)$ from Equation 6-2

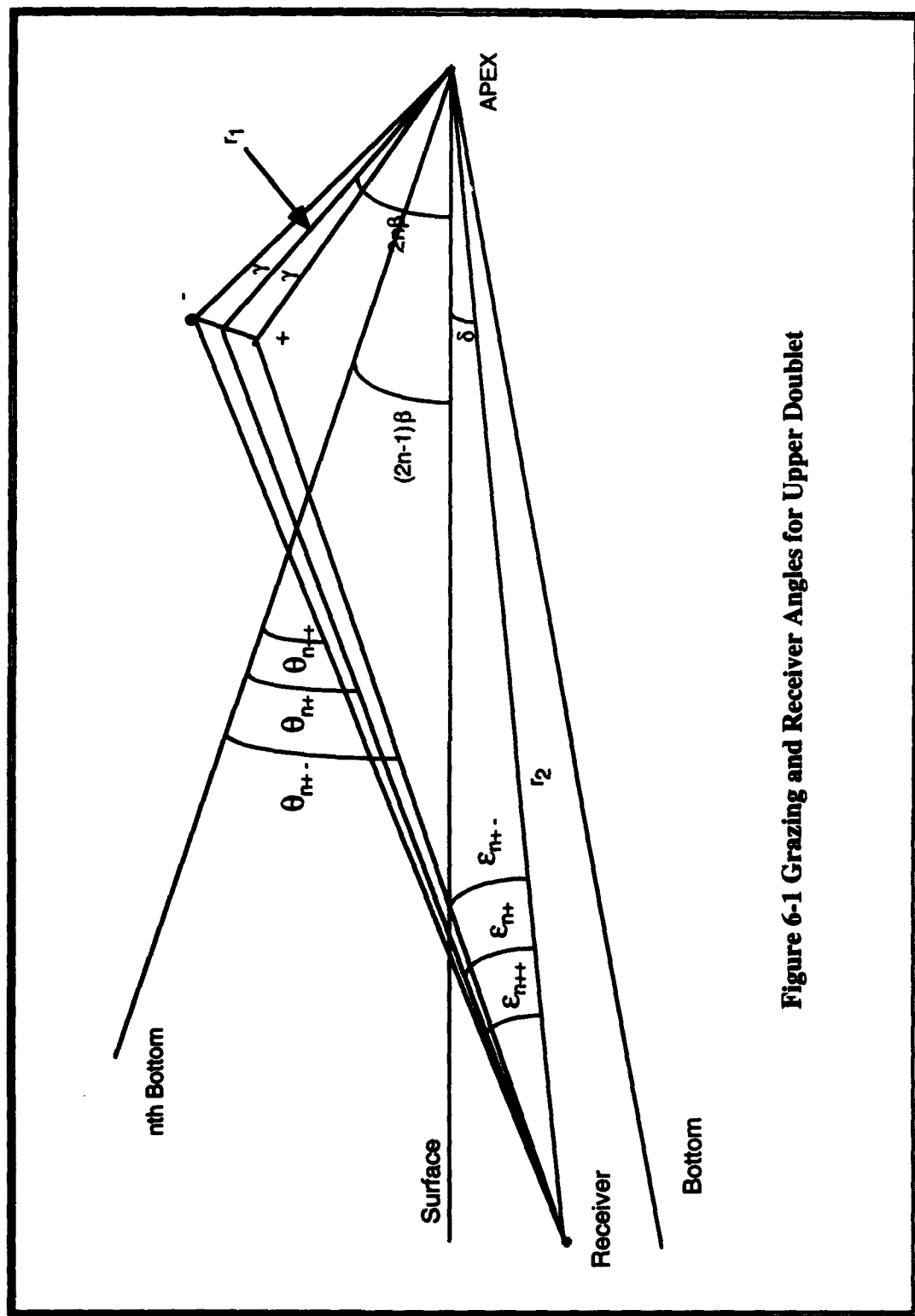


Figure 6-1 Grazing and Receiver Angles for Upper Doublet

$$\epsilon_{n\pm} = \epsilon_n \pm \frac{r_1}{r_{n\pm}} \gamma \cos(2n\beta + \delta) \quad (6-6)$$

for the upper half space and

$$\epsilon_{n\pm} = \epsilon_n \pm \frac{r_1}{r_{n-}} \gamma \cos(2n\beta - \delta) \quad (6-7)$$

for the lower half space.

B. ANGLE OF INCIDENCE FOR UPPER AND LOWER DOUBLET IMAGES

The angle from the surface to each virtual bottom is

$$\theta_{no} = (2n-1)\beta \quad (6-8)$$

The angle of incidence of the doublet midpoint is

$$\theta_{n\pm} = (2n-1)\beta \pm \delta + \epsilon \quad (6-9)$$

The angles of incidence with the virtual bottom is different with each upper and lower doublet image. The angles of incidence for the upper half space are given by

$$\theta_{n\pm} = (2n-1)\beta + \delta + \epsilon_{n\pm} \quad (6-10)$$

By substituting Equation 6-5 into Equation 6-10 and making the standard small angle assumptions

$$\theta_{n\pm} = (2n-1)\beta + \delta + \frac{r_1}{r_{n\pm}} [\sin(2n\beta + \delta)(1) \pm \gamma \cos(2n\beta + \delta)] \quad (6-11)$$

Expanding the sine term and making the standard small angle assumptions again

$$\theta_{n\pm} = (2n-1)\beta + \delta + \frac{r_1}{r_{n\pm}} [\sin(2n\beta)(1) + \delta \cos(2n\beta) \pm \gamma \cos(2n\beta + \delta)] \quad (6-12)$$

Rearranging the terms result in

$$\theta_{n\pm} = (2n-1)\beta + \frac{r_1}{r_{n+}} \sin(2n\beta) + \delta \left[1 + \frac{r_1}{r_{n+}} \cos(2n\beta) \right] \pm \frac{r_1}{r_{n+}} \gamma \cos(2n\beta + \delta) \quad (6-13)$$

An assumption can be made that if $r_1 \ll r_{n+}$, the sine term in the above equation is small so the it can be neglected. The result of Equation 6-13 is

$$\theta_{n\pm} = \theta_{no} + \delta \left[1 + \frac{r_1}{r_{n+}} \cos(2n\beta) \right] \pm \frac{r_1}{r_{n+}} \gamma \cos(2n\beta + \delta) \quad (6-14)$$

The equivalent equation for the lower half space is

$$\theta_{n\pm} = \theta_{no} + \delta \left[1 + \frac{r_1}{r_n} \cos(2n\beta) \right] \pm \frac{r_1}{r_n} \gamma \cos(2n\beta - \delta) \quad (6-15)$$

Expanding the cosine term results in

$$\theta_{n\pm} = \theta_{no} + \delta \left[1 + \frac{r_1}{r_{n+}} \cos(2n\beta) \right] \pm \frac{r_1}{r_{n+}} \gamma [\cos(2n\beta)\cos(\delta) - \sin(2n\beta)\sin(\delta)] \quad (6-16)$$

Using the standard small angle approximations and assuming the sine term is small

$$\theta_{n\pm} = \theta_{no} + \delta \left[1 + \frac{r_1}{r_{n+}} \cos(2n\beta) \right] \pm \frac{r_1}{r_{n+}} \gamma \cos(2n\beta) \quad (6-17)$$

for the upper half-space and

$$\theta_{n\pm} = \theta_{no} + \delta \left[1 + \frac{r_1}{r_{n-}} \cos(2n\beta) \right] \pm \frac{r_1}{r_{n-}} \gamma \cos(2n\beta) \quad (6-18)$$

for the lower half-space.

C. AMPLITUDES

The amplitude of each image in the quadruplet needs to be calculated due to their differences. The coefficients of Equation 6-17 and 6-18 are used where

$$a_n = 1 + \frac{r_1}{r_n} \cos(2n\beta) \quad (6-19)$$

and

$$b_n = \frac{r_1}{r_n} \cos(2n\beta) \quad (6-20)$$

The reflection coefficient can now be written for each image

$$R_{n\pm} = R_n e^{-n\alpha\Delta r} \quad (6-21)$$

expanding the above equation and using the sine approximation for an angle

$$R_{n\pm} = R_n e^{-n\alpha\Delta r} e^{\pm n\alpha\gamma\phi_n} \quad (6-22)$$

Each of the image amplitudes can now be expressed

$$\begin{aligned} A_{n-} &= R_n e^{-n\alpha a_n \delta} e^{-n\alpha b_n \gamma} & B_{n-} &= R_n e^{n\alpha a_n \delta} e^{n\alpha b_n \gamma} \\ A_{n+} &= R_n e^{-n\alpha a_n \delta} e^{n\alpha b_n \gamma} & B_{n+} &= R_n e^{n\alpha a_n \delta} e^{-n\alpha b_n \gamma} \end{aligned} \quad (6-23)$$

Using Equation 3-11 and the definition of

$$\cosh(x) = \frac{e^x + e^{-x}}{2} \quad \sinh(x) = \frac{e^x - e^{-x}}{2} \quad (6-24)$$

where $x = n\alpha b_n \delta$ gives

$$\begin{aligned} \Delta A_n &= R_n \sinh(n\alpha b_n \delta) e^{n\alpha a_n \delta} & \Delta B_n &= R_n \sinh(n\alpha b_n \delta) e^{n\alpha a_n \delta} \\ A_n &= R_n \cosh(n\alpha b_n \delta) e^{n\alpha a_n \delta} & B_n &= R_n \cosh(n\alpha b_n \delta) e^{n\alpha a_n \delta} \end{aligned} \quad (6-25)$$

The equations combine to form

$$\frac{\Delta A}{A_n} = \tanh(n\alpha b_n \gamma) \quad \frac{\Delta B}{B_n} = \tanh(n\alpha b_n \gamma) \quad (6-26)$$

Now the full quadruplet equation can be written as

$$\begin{aligned}
\mathbf{P} = P_o + \sum_{n=1}^N \frac{2j}{r_n} \mathbf{R}_n \cosh(n\alpha b_n \gamma) e^{-(\alpha x - kr)} e^{-j\phi} \\
\begin{bmatrix} e^{-n\alpha a_n \delta - j\mu d} (\sin(kr_1 \gamma \sin(2n\beta + \delta)) - j \tanh(n\alpha b_n \gamma) \cos(kr_1 \gamma \sin(2n\beta + \delta))) \\ -e^{-n\alpha a_n \delta + j\mu d} (\sin(kr_1 \gamma \sin(2n\beta - \delta)) - j \tanh(n\alpha b_n \gamma) \cos(kr_1 \gamma \sin(2n\beta - \delta))) \end{bmatrix}
\end{aligned}$$

(6-27)

where $P_o = \frac{2j}{r} \sin(kr_1 \gamma \delta)$.

VII. PROCEDURE AND RESULTS

This thesis had three objectives:

1. Convert the WEDGE/URTEXT to MATLAB™ and test it in all cases (slow and fast bottom, cross-slope, and with bottomloss).
2. Linearize the quadruplet expansion code by Joyce [Ref. 27]
3. Extend the quadruplet expansion to the fast bottom case with a approximation of the Rayleigh reflection coefficient.

A. CONVERT WEDGE/URTEXT TO MATLAB

The image model baseline program is called WEDGE. It is written in GWBASIC by Professor A. B. Coppens and is run on a IBM XT(8088) desktop computer. WEDGE was translated into FORTRAN by Nassopoulos [Ref. 25]. It was renamed URTEXT and is on the mainframe computer at the Naval Postgraduate School. Translating it to a language that is fast and can be run on a high performance desktop computer or workstation was necessary to make WEDGE data readily available for comparison to the quadruplet expansion. MATLAB™ [Ref. 31] was chosen because it is a high level scripting language which runs on a variety of computer operating systems including VAX, MS-DOS, UNIX, and Macintosh and that it is the mathematics program that the author is most familiar with.

Validation of the MATLAB™ version of WEDGE, called WEDGEMAT, was conducted by comparing the results of WEDGE and URTEXT to those of WEDGEMAT.

Tables 7-1, through 7-4 show the results of the comparison of URTEXT with WEDGEMAT_{tr}. WEDGEMAT_{tr} is the a version of WEDGE that ends the calculation process when the pressure amplitude is less than 0.00000001. The major error at the

surface is due to the difference in precision of the different languages. FORTRAN uses single precision variables, accurate to six decimal places. MATLAB™ is precise to 13 places, therefore at the small pressures near the surface the round-off errors are extreme. It should be noted that the results of Nassoloulos are normalized pressures where the actual pressure is multiplied by the source scaling distance r_1 .

Tables 7-5 through 7-8 show the comparison of WEDGE to WEDGEMATtr. The WEDGE program in GWBASIC uses variables precise to 12 decimal places so it compares more favorably with the MATLAB version. Runs were done with fast bottoms, bottomloss, and cross-slope to test accuracy. The results are very favorable.

A run was made on an 10° slope with the data taken from the surface to bottom sampled every 0.05° . Figure 7-1 shows pressure falls off linearly as the sound nears the surface (bottom of graph). This implies the model is valid at the surface.

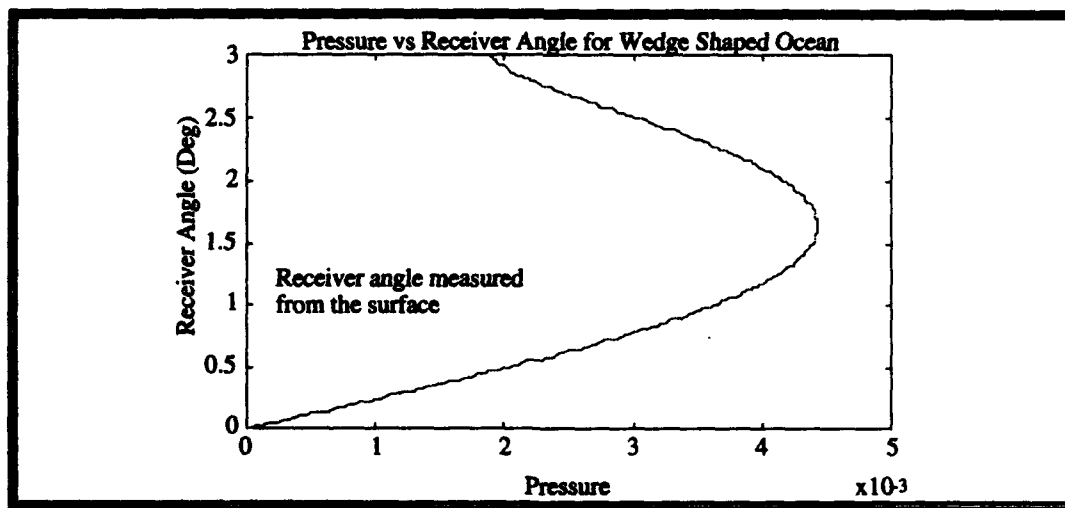


Figure 7-1 - Pressure vs. Receiver Angle

WEDGEMATtr has undergone basic proofing. When compared with previous versions in FORTRAN and GWBASIC, it is more flexible both in platforms run, model

variables, and speed. Most importantly, now it can be used to check the quadruplet expansion data to verify results.

**TABLE 7-1 SLOW BOTTOM COMPARISON OF URTEXT AND
WEDGEMATTR**

$\beta=3$ $\gamma=1$ $r_1=1$ $r_2=10$ $y_0=0$ $\rho_1/\rho_2=0.9$

$c_1=1500\text{m/s}$ $c_2=1475\text{m/s}$ $\alpha/k_2=0$

Receiver Angle	Pressure Amplitude			Phase Angle		
	Image		Absolute	Image		Absolute
	Theory	MATLAB	Difference	Theory	MATLAB	Difference
0.03°	0.000123	0.000126	0.000003	-54.7°	-48.8°	5.9°
0.30°	0.001255	0.001250	0.000005	-49.8°	-48.7°	1.1°
0.60°	0.002415	0.002400	0.000015	-48.8°	-48.5°	0.3°
0.90°	0.003352	0.003356	0.000004	-49.4°	-48.1°	1.3°
1.20°	0.004028	0.004039	0.000011	-48.5°	-47.5°	1.0°
1.50°	0.004384	0.004390	0.000006	-47.5°	-46.4°	1.1°
1.80°	0.004369	0.004377	0.000008	-45.7°	-44.5°	1.2°
2.10°	0.004010	0.004002	0.000008	-42.1°	-41.1°	1.0°
2.40°	0.003339	0.003316	0.000023	-35.2°	-34.5°	0.7°
2.70°	0.002471	0.002467	0.000004	-20.8°	-19.7°	1.1°
	Avg Pressure Diff= 0.000008			Avg Phase Diff = 1.5°		

Note: Normalized pressure equation used where $P = r_1 \sqrt{P_l^2 + P_u^2}$

**TABLE 7-2 SLOW BOTTOM COMPARISON OF URTEXT AND
WEDGEMATTR**

$\beta=4$ $\gamma=1$ $r_1=5$ $r_2=12$ $y_0=0$ $\rho_1/\rho_2=0.7$

$c_1=1500\text{m/s}$ $c_2=1420\text{m/s}$ $\alpha/k_2=0$

Receiver Angle	Pressure Amplitude			Phase Angle		
	Image		Absolute	Image		Absolute
	Theory	MATLAB	Difference	Theory	MATLAB	Difference
0.04°	0.040927	0.041003	0.000076	-149.3°	-149.1°	0.2°
0.40°	0.394236	0.394324	0.000088	-148.6°	-148.5°	0.1°
0.80°	0.701851	0.701860	0.000009	-146.5°	-146.3°	0.2°
1.20°	0.873027	0.873049	0.000022	-142.3°	-142.2°	0.1°
1.60°	0.915180	0.915294	0.000114	-135.2°	-135.1°	0.1°
2.00°	0.887048	0.887038	0.000010	-124.6°	-124.5°	0.1°
2.40°	0.851987	0.851901	0.000086	-112.8°	-112.7°	0.1°
2.80°	0.810276	0.810180	0.000096	-104.5°	-104.4°	0.1°
3.20°	0.704744	0.704662	0.000112	-103.6°	-103.5°	0.1°
3.60°	0.503485	0.503407	0.000078	-115.2°	-115.0°	0.2°
	Avg Pressure Diff= 0.000069			Avg Phase Diff = 0.1°		

Note: Normalized pressure equation used where $P = r_1 \sqrt{P_i^2 + P_u^2}$

**TABLE 7-3 SLOW BOTTOM COMPARISON OF URTEXT AND
WEDGEMATTR**

$\beta=5 \quad \gamma=4 \quad r_1=2 \quad r_2=400 \quad y_0=0 \quad \rho_1/\rho_2=0.6$

$c_1=1500\text{m/s} \quad c_2=1410\text{m/s} \quad \alpha/k_2=0$

Receiver Angle	Pressure Amplitude			Phase Angle		
	Image		Absolute	Image		Absolute
	Theory	MATLAB	Difference	Theory	MATLAB	Difference
0.05°	0.000087	0.000082	0.000005	56.3°	65.2°	8.9°
0.50°	0.000818	0.000812	0.000006	62.6°	65.3°	2.7°
1.00°	0.001532	0.001549	0.000017	62.2°	65.4°	3.2°
1.50°	0.002151	0.002144	0.000007	63.0°	65.5°	2.5°
2.00°	0.002537	0.002542	0.000005	62.6°	65.6°	3.0°
2.50°	0.002704	0.002704	0	63.3°	65.7°	2.4°
3.00°	0.002639	0.002613	0.000026	63.0°	65.8°	2.8°
3.50°	0.002276	0.002268	0.000006	62.4°	65.9°	3.5°
4.00°	0.001699	0.001690	0.000009	63.0°	65.8°	2.8°
4.50°	0.000926	0.000916	0.000010	60.5°	65.1°	5.1°
	Avg Pressure Diff= 0.000009			Avg Phase Diff = 3.7°		

Note: Normalized pressure equation used where $P = r_1 \sqrt{P_I^2 + P_u^2}$

**TABLE 7-4 SLOW BOTTOM COMPARISON OF URTEXT AND
WEDGEMATTR**

$\beta=6$ $\gamma=2$ $r_1=0.8$ $r_2=5$ $y_0=0$ $\rho_1/\rho_2=0.8$

$c_1=1500\text{m/s}$ $c_2=1450\text{m/s}$ $\alpha/k_2=0$

Receiver Angle	Pressure Amplitude			Phase Angle		
	Image	Absolute		Image	Absolute	
	Theory	MATLAB	Difference	Theory	MATLAB	Difference
0.06°	0.000372	0.000377	0.000005	-50.2°	-48.3°	1.9°
0.60°	0.003728	0.003726	0.000002	-48.9°	-48.6°	0.3°
1.20°	0.007214	0.007205	0.000009	-49.9°	-49.8°	0.1°
1.80°	0.010212	0.010210	0.000002	-52.2°	-52.0°	0.2°
2.40°	0.012559	0.012557	0.000002	-55.3°	-55.3°	0°
3.00°	0.014134	0.014136	0.000002	-60.2°	-60.1°	0.1°
3.60°	0.014946	0.014947	0.000001	-67.1°	-66.0°	1.1°
4.20°	0.015168	0.015166	0.000002	-77.0°	-76.8°	0.2°
4.80°	0.015224	0.015224	0	-90.5°	-90.4°	0.1°
5.40°	0.015831	0.015832	0.000001	-107.7°	-107.6°	0.1°
	Avg Pressure Diff= 0.000003			Avg Phase Diff = 0.4°		

Note: Normalized pressure equation used where $P = r_1 \sqrt{P_l^2 + P_u^2}$

**TABLE 7-5 FAST BOTTOM COMPARISON OF WEDGE AND
WEDGEMATTR WITH BOTTOMLOSS**

$\beta=3$ $\gamma=1$ $r_1=1$ $r_2=10$ $y_0=0$ $\rho_1/\rho_2=0.9$

$c_1=1500\text{m/s}$ $c_2=1666\text{m/s}$ $\alpha/k_2=0.0001$

Receiver Angle	Pressure Amplitude			Phase Angle		
	Image Theory	Absolute MATLAB	Absolute Difference	Image Theory	Absolute MATLAB	Absolute Difference
0.03°	0.01256	0.01255	0.00001	-3.1°	-3.1°	0
0.30°	0.12379	0.12377	0.00002	-3.3°	-3.3°	0
0.60°	0.23680	0.23681	0.00001	-3.8°	-3.9°	0.1°
0.90°	0.32981	0.32982	0.00001	-4.9°	-4.9°	0
1.20°	0.39269	0.39272	0.00003	-6.2°	-6.2°	0
1.50°	0.42213	0.42214	0.00001	-8.9°	-8.8°	0.1°
1.80°	0.40586	0.40585	0.00001	-10.7°	-10.6°	0.1°
2.10°	0.34833	0.34832	0.00001	-16.6°	-16.7°	0.1°
2.40°	0.24512	0.24513	0.00001	-15.6°	-15.7°	0.1°
2.70°	0.14819	0.14816	0.00003	-13.5°	-13.5°	0
	Avg Pressure Diff= 0.00002			Avg Phase Diff = 0.5°		

**TABLE 7-6 FAST BOTTOM COMPARISON OF WEDGE AND
WEDGEMATTR WITH BOTTOMLOSS**

$\beta=3$ $\gamma=1$ $r_1=1$ $r_2=100$ $y_0=0$ $\rho_1/\rho_2=0.9$

$c_1=1500\text{m/s}$ $c_2=1875\text{m/s}$ $\alpha/k_2=0.0001$

Receiver Angle	Pressure Amplitude			Phase Angle		
	Image Theory	Absolute MATLAB	Absolute Difference	Image Theory	Absolute MATLAB	Absolute Difference
0.03°	0.00210	0.00199	0.00011	35.4°	40.3°	4.9°
0.30°	0.02069	0.02062	0.00007	34.9°	35.4°	0.5°
0.60°	0.03962	0.03966	0.00004	34.8°	34.9°	0.1°
0.90°	0.05529	0.05535	0.00006	34.5°	34.5°	0
1.20°	0.06632	0.06640	0.00008	34.1°	34.1°	0
1.50°	0.07174	0.07183	0.00009	33.6°	33.6°	0
1.80°	0.07095	0.07105	0.00010	33.1°	33.1°	0
2.10°	0.06385	0.06394	0.00009	32.7°	32.7°	0
2.40°	0.05088	0.05093	0.00005	33.5°	33.4°	0.1°
2.70°	0.02783	0.02782	0.00001	38.9°	38.9°	0
	Avg Pressure Diff= 0.00006			Avg Phase Diff = 0.6°		

**TABLE 7-7 FAST BOTTOM COMPARISON OF WEDGE AND
WEDGEMATTR IN CROSS-SLOPE WITH BOTTOMLOSS**

$\beta=3$ $\gamma=1$ $r_1=1$ $r_2=10$ $y_0=4$ $\rho_1/\rho_2=0.9$

$c_1=1500\text{m/s}$ $c_2=1666\text{m/s}$ $\alpha/k_2=0.0001$

Receiver Angle	Pressure Amplitude			Phase Angle		
	Image Theory	Absolute MATLAB	Difference	Image Theory	Absolute MATLAB	Difference
0.03°	0.01024	0.01094	0.00070	-44.3°	-43.2°	1.1°
0.30°	0.10162	0.10227	0.00065	-44.2°	-44.3°	0.1°
0.60°	0.19699	0.19716	0.00015	-44.3°	-44.2°	0.1°
0.90°	0.27908	0.27931	0.00022	-44.5°	-44.6°	0.1°
1.20°	0.34418	0.34418	0	-44.8°	-44.8°	0
1.50°	0.39920	0.39896	0.00024	-44.8°	-44.9°	0.1°
1.80°	0.40001	0.39954	0.00047	-39.2°	-39.3°	0.1°
2.10°	0.35816	0.35799	0.00017	-37.5°	-37.5°	0
2.40°	0.27680	0.27659	0.00021	-34.5°	-34.6°	0.1°
2.70°	0.17050	0.17036	0.00014	-33.2°	-33.2°	0
	Avg Pressure Diff= 0.00029			Avg Phase Diff = 0.2°		

**TABLE 7-8 FAST BOTTOM COMPARISON OF WEDGE AND
WEDGEMATTR IN CROSS-SLOPE WITH BOTTOMLOSS**

$$\beta=3 \quad \gamma=0.5 \quad r_1=1 \quad r_2=10 \quad y_0=8 \quad \rho_1/\rho_2=0.9$$

$$c_1=1500\text{m/s} \quad c_2=1666\text{m/s} \quad \alpha/k_2=0.0001$$

Receiver Angle	Pressure Amplitude			Phase Angle		
	Image Theory	Absolute MATLAB	Absolute Difference	Image Theory	Absolute MATLAB	Absolute Difference
0.03°	0.00493	0.00501	0.00008	-33.4°	-27.4°	6.0°
0.30°	0.04887	0.04911	0.00024	-33.4°	-33.0°	0.4°
0.60°	0.09466	0.09495	0.00029	-33.5°	-33.4°	0.1°
0.90°	0.013453	0.13463	0.00010	-33.5°	-33.6°	0.1°
1.20°	0.16917	0.16949	0.00032	-34.7°	-34.6°	0.1°
1.50°	0.18791	0.18845	0.00054	-29.0°	-28.9°	0.1°
1.80°	0.18490	0.18554	0.00064	-27.8°	-27.8°	0
2.10°	0.16321	0.16382	0.00061	-24.6°	-24.6°	0
2.40°	0.12657	0.12706	0.00049	-23.4°	-23.5°	0.1°
2.70°	0.07764	0.07792	0.00028	-21.8°	-21.9°	0.1°
	Avg Pressure Diff= 0.00036			Avg Phase Diff = 0.7°		

B. LINEARIZATION OF QUADRUPLLET EXPANSION PROGRAM

The original quadruplet expansion program was written by Joyce [Ref. 27]. His program is used as a basis for the fast bottom case examined later in this chapter. The linearized program is in Appendix A-1 and A-2 and has incorporated into it the fast bottom, reflection coefficients of Equations 7-1 and 5-28.

The original quadruplet expansion code used "For Loops" to compute its products. The code was linearized to speed processing time. A speed factor of 8 was achieved with the same output results [Ref. 27]. Table 7-9 shows relative execution time for a 3° wedge. This table is only meant to give the reader a 'feel' of the time involved in running the programs. The WEDGE program in GWBASIC was run on a IBM XT (8088) with FPU. All other programs were run on a Mac IIsi (68030 @ 20 MHz) with Applied Engineering 32k RAM cache card (with 20 MHz FPU) using MATLAB™ 3.5.

TABLE 7-9 EXECUTION TIME OF IMAGE PROGRAMS

Bottom Type	WEDGE (truncated version)	WEDGEMAT	WEDGEMATtr	QUAD	Linearized QUAD
Slow	16s	42s	2s	8s	1s
Fast	124s	43s	5s	8s	1s

Another method to speed calculation is to use the "For Loop" and put in a "Break" command to stop the calculation process after the pressure for a certain image or image doublets, in the quadruplet case, falls below a specified level. This was done in the WEDGE (truncated version) and WEDGEMATtr. This especially useful in a slow bottom case where the first 3 of 30 quadruplets (for a 3° wedge) would be 98 percent of the amplitude. This idea was not explored for the quadruplet expansion case.

C. FAST BOTTOM REFLECTION COEFFICIENT APPROXIMATION

The Rayleigh reflection coefficient without absorption is

$$R_{nm} = \frac{\frac{\rho_2 c_2}{\rho_1 c_1} + j \frac{\sqrt{\left(\frac{c_2}{c_1}\right)^2 \cos^2(\theta_{nm}) - 1}}{\sin(\theta_{nm})}}{\frac{\rho_2 c_2}{\rho_1 c_1} - j \frac{\sqrt{\left(\frac{c_2}{c_1}\right)^2 \cos^2(\theta_{nm}) - 1}}{\sin(\theta_{nm})}} \quad (7-1)$$

can be approximated by Equation 5-28 which is

$$R_{nm} = -e^{-2j \tan^{-1}\left(\frac{bx}{\sqrt{1-x^2}}\right)}$$

For a fast bottom 3° wedge with the following parameters

$$c_1 = 1500m / s$$

$$\rho_1 = 1Kg / m^3$$

$$c_2 = 1666m / s$$

$$\rho_2 = 1.1111Kg / m^3$$

the reflection coefficients are displayed in Table 7-10. In a 3° wedge, 30 reflection coefficients would be calculated. A fast bottom requires the first 10 terms since the cumulative product is multiplied with the amplitude of the quadruplet. The cumulative product after the tenth term is very small and contributes little to the final pressure as can be seen in Figure 5-1.

**TABLE 7-10 COMPARISON OF RAYLEIGH AND ARCTAN
APPROXIMATION REFLECTION COEFFICIENTS**

Quad Number	Rayleigh Reflection Coefficient		Tan ⁻¹ Approximation	
	Amp	Phase	Amp	Phase
1	1	149.7°	1	149.3°
2	1	121.2°	1	117.8°
3	1	95.1°	1	83.7°
4	1	70.9°	1	38.3°
5	1	46.1°	0.380	0
6	0.9084	0	0.2471	0
7	0.4839	0	0.1885	0
8	0.3750	0	0.1568	0
9	0.3120	0	0.1375	0
10	0.2669	0	0.1251	0

The correlation of the two reflection coefficients are good until the third quadruplet. Then the Tan⁻¹ approximation fall off much more quickly than the Rayleigh values. This can be seen in the complex plane plot of the reflection coefficients in Figure 7-2. The first five reflection coefficients are numbered in each case.

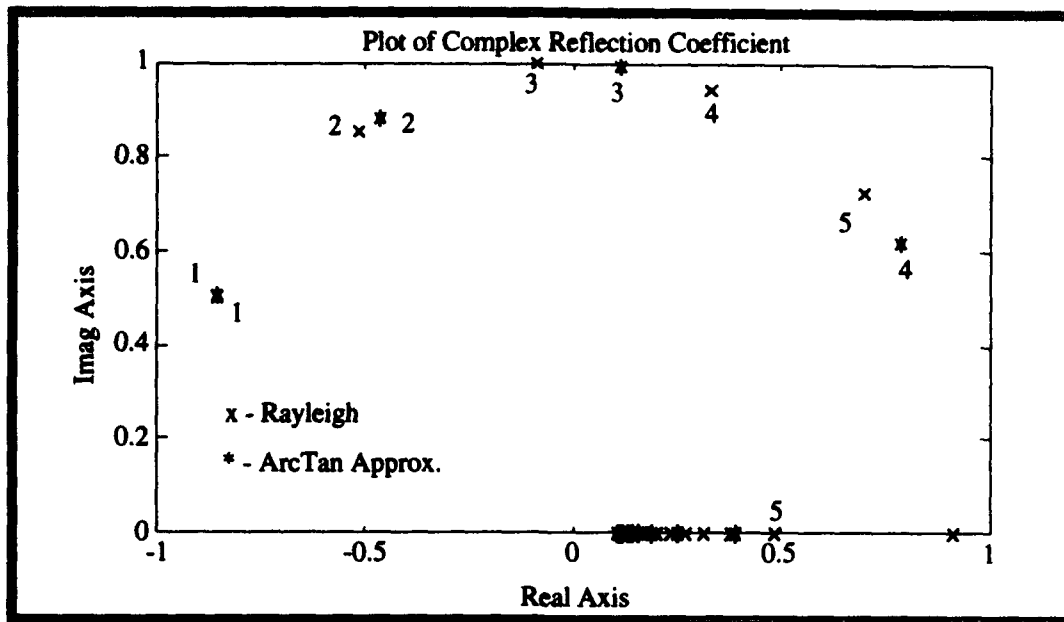


Figure 7-2 - Comparison of Complex Reflection Coefficients

**TABLE 7-11 COMPARISON OF THE CUMULATIVE RAYLEIGH AND
ACTTAN APPROXIMATION REFLECTION COEFFICIENTS**

Quad Number	Rayleigh Reflection Coefficient		Tan ⁻¹ Approximation	
	Amp	Phase	Amp	Phase
1	1	149.7°	1	149.3°
2	1	-89.1°	1	-92.9°
3	1	6.1°	1	-9.2°
4	1	77.0°	1	29.0°
5	1	123.1°	0.3880	29.0°
6	0.9084	123.1°	0.0959	29.0°
7	0.4396	123.1°	0.0181	29.0°
8	0.1648	123.1°	0.0028	29.0°

The most important factor is the cumulative reflection coefficient which is shown in Table 7-11. There is a wide disparity between the actual and approximated reflection coefficients. The correlation is good until the second quadruplet, then the products diverge. The reason for this is the inaccuracy of each grazing with the bottom is amplified by the complex multiplication of the cumulative product.

A test was run comparing the amplitude and phase at the receiver. The output is displayed in Table 7-12. Data were taken from the surface to the bottom in 0.5° increments. The differences are attributed to the inaccuracy of the reflection coefficient after the second quadruplet. With the fast bottom, the equations are very sensitive to the phase of the reflection coefficients. Even though the reflection coefficients have an amplitude of 1, the phase can cause constructive and destructive interference. Also with a fast bottom, many of the terms in the quadruplet expansion are complex there by magnifying the effect of the phase inaccuracy.

**TABLE 7-12 COMPARISON OF AMPLITUDE AND PHASE OF USING
RAYLEIGH AND ARCTAN APPROXIMATION**

Receiver Angle (from Surface) δ	Rayleigh Reflection Coefficient		Tan ⁻¹ Approximation	
	Amp	Phase	Amp	Phase
0°	0	0	0	0
0.5°	0.0082	173.0°	0.0025	-83.3°
1.0°	0.0164	172.9°	0.0049	-83.2°
1.5°	0.0245	172.7	0.0074	-83.1°
2.0°	0.0239	172.4°	0.0070	-82.8
2.5°	0.0161	172.1°	0.0043	-82.1°
3.0°	0.0010	162.2°	0.0006	-65.6°

Now one still has to compare the results of WEDGEMAT_{tr}, to the quadruplet expansion. The quadruplet expansion with the Rayleigh reflection coefficient was tested in the same conditions as in the above table. The results are displayed in Table 7-13.

TABLE 7-13 COMPARISON OF AMPLITUDE AND PHASE OF QUADRUPLLET EXPANSION USING RAYLEIGH AND IMAGE MODEL

Receiver Angle (from Surface) δ	Rayleigh Reflection Coefficient		WEDGEMAT _{tr}	
	Amp	Phase	Amp	Phase
0°	0	0	0	0
0.5°	0.0082	173.0°	0.0328	-12.3°
1.0°	0.0164	172.9°	0.0592	-12.6°
1.5°	0.0245	172.7	0.0747	-12.6°
2.0°	0.0239	172.4°	0.0720	-5.7
2.5°	0.0161	172.1°	0.0425	-1.5°
3.0°	0.0010	162.2°	0.0019	19.0°

The comparison of the image model (WEDGEMAT_{tr}) and the quadruplet expansion using the Rayleigh reflection coefficient reveals an error factor of about 3 in amplitude. This can be attributed to the many approximations made in deriving the equation for the quadruplet expansion which was covered in Chapter III to VI of this thesis. Many of the approximations are first order and are not good enough to get accurate results.

The quadruplet expansion using the exponential approximation for a slow bottom [Ref. 27] is limited to small wedge angle, the source close to the surface, and the receiver must be in the 'far field'. The reason for the limitation to a small wedge angle ($\beta \sim 3$) is to minimize the errors in the small angle approximation ($\cos(\gamma) \approx 1$ and $\sin(\delta) \approx \delta$). The source needs to be close to the surface (upper half of the wedge) so the distance between

the upper and lower doublet pairs are reasonably close. The 'far field' requires $r_n \gg r_1$, which is about 50 dump distances (X_c). The reason for this is to insure the receiver angle (ϵ) is small and the difference between the upper and lower images in the doublet are very small. These requirements are needed to insure that in the slow bottom case, where the reflection coefficient is real, and the cumulative product of the reflection coefficient is ~ 0 by the third quadruplet (of 30) in a 3° wedge. In the fast bottom case, when the terms are complex and phase dependent, the cumulative reflection coefficient will go to ~ 0 by the ninth or tenth quadruplet. in this latter case there are many more complex operations being executed thereby magnifying the need for accurate approximations of the reflection coefficients and the terms in the quadruplet expression (Equation 6-27).

VIII. CONCLUSION AND RECOMMENDATIONS

Image theory is an ideal method for calculating the transmission loss in a shallow water (wedge shaped ocean) environment. It can be used in cross-slope, at all frequencies and in transitional cut off regions that are out of bounds for normal mode theories.

This thesis has successfully converted the GWBASIC and FORTRAN code of WEDGE and URTEXT to MATLAB™, which is a high level scripting language. The original WEDGE program is accurate in fast and slow bottoms, cross-slope, and with bottomloss. The WEDGEMAT program retains all the same qualities but is much faster to run. The quadruplet expansion program for a slow bottom by Joyce [Ref. 27] was linearized to increase processing speed by a factor of 8 while retaining the same results.

This thesis also incorporated a \tan^{-1} approximation of the reflection coefficient for a fast bottom into the quadruplet expansion. Due to the inaccuracy of the reflection coefficient after the second quadruplet, the results were not favorable. It was also discovered that even with an accurate Rayleigh reflection coefficient, the first order approximations made in developing the quadruplet expansion equation (Equation 6-27) are not accurate enough for the fast bottom case.

The next steps in this area of research is to find a better approximation for the fast bottom reflection coefficient and to increase the accuracy of the terms of the quadruplet expansion equation (Equation 6-27).

APPENDIX A-1

```

%
% QUADATAN
% Linearized Quadruplet Expansion of Method
% of Images. Based on PQUAD.m by Joyce.
%
% This program will provide pressure amplitude and
% the phase angle at the reciever. All distances are
% ratios of dump distances Xc. All angles are inputed
% in degrees. This model includes Rayleigh Reflection
% coefficient for fast bottom case and exponential
% approximation for slow bottom case.
%
% By Pat Takamiya
%
clear; clc; clg;
% Input Parameters
B=input('Enter bottom wedge angle in deg (beta) =');
G=input('Enter source angle from surface in deg (gamma) =');
D=input('Enter receiver angle from surface in deg (delta)=');
d1=input('Enter Density ratio, water to bottom =');
CC=input('Enter sound speed ratio, water to bottom =');
r1=input('Enter range of source from apex (r1) =');
r2=input('Enter range of receiver from apex (r2) =');
y0=0;
%
% Determine Number of Image Quadruplets
% Convert Angles from Deg to Rads
N1=fix(90/B);
B=B*(pi/180);
G=G*(pi/180);
D=D*(pi/180);
%
% Determine Scaling for Fast or Slow Bottoms
tqq=tan(B);
    if CC<1                                % Fast Bottom
        tqq1=acos(CC);
        tqq2=sin(tqq1);
    else
        tqq1=acos(1/CC);    % Slow Bottom
        tqq2=tan(tqq1);
    end
tqq3=2*tqq2*tqq;
t4=pi/tqq3;                                % Scaled wave number

```

```

%
% Calculate Constants and Primary Doublet
%
alpha=2*(1/d1)/(sqrt((CC^2)-1));
r=sqrt((r1^2)+(r2^2)+(y0^2)-(2*r1*r2*cos(D)));
r3=abs(r2-r1);
r4=r1*r2/(r3^2);
mu=r2/r3;
q=t4*r1*G*D;
p1=(2/r)*sin(q);
f=0;
%
% Quadruplet Summation
%
n=(1:N1);
    s(n)=n;
    th(n)=2*n*B;
    d(n)=t4*r1*D*sin(th(n));
    phi(n)=t4*r1*mu*(1-cos(th(n)));
% Reflection Coeff
    ru(n)=sqrt((r1^2)+(r2^2)+(y0^2)-2*r1*r2*cos(th(n)+D));
    rl(n)=sqrt((r1^2)+(r2^2)+(y0^2)-2*r1*r2*cos(th(n)-D));
    r5(n)=r1./ru(n);
    r6(n)=r1./rl(n);
    a1(n)=1-r5(n).*cos(th(n));
    b1(n)=r6(n).*cos(th(n));
    if CC>1
        rr(n)=(B*alpha.*(n.^2));
        R(n)=-exp(-rr(n));
    else
        rc=(1/CC)*1/d1;
        cc1=1/CC;
        g1(n)=sqrt(cc1*cc1*cos(th(n))-1);
        g2(n)=sin(th(n));
        g3(n)=j*g1(n)./g2(n);
        R1(n)=(rc+g3(n))./(rc-g3(n));
        R(n)=cumprod(-R1(n));
    end

    a(n)=n.*alpha*D.*a1(n);
    b(n)=n.*alpha*G.*b1(n);
%
% Pressure
    u1(n)=cosh(b(n));
    u2(n)=exp(-j*phi(n));
    u3(n)=(-2/r).*R(n).*u1(n).*u2(n);
%

```

```

% Upper Image
v1(n)=sin(th(n)+D);
v2(n)=t4*r1*G*v1(n);
v3(n)=sin(v2(n));
v4(n)=cos(v2(n));
v5(n)=-a(n)-j*mu*d(n);
v6(n)=exp(v5(n));
v7(n)=tanh(b(n));
v8(n)=v6(n).*(v3(n)-j*v7(n).*v4(n));

%
% Lower Image
w1(n)=sin(th(n)-D);
w2(n)=t4*r1*G*w1(n);
w3(n)=sin(w2(n));
w4(n)=cos(w2(n));
w5(n)=a(n)+j*mu*d(n);
w6(n)=exp(w5(n));
w7(n)=w6(n).*(w3(n)-j.*v7(n).*w4(n));

%
% Summation
p(n)=u3(n).*(v8(n)-w7(n));
p2=sum(p(n));
%
%
ps=p1+p2;
ph1=atan2(imag(ps),real(ps));
phase=180*ph1/pi
P=sqrt(real(ps)^2 + imag(ps)^2)

```

APPENDIX A-2

```
%  
% QUADATAN  
% Linearized Quadruplet Expansion of Method  
% of Images. Based on PQUAD.m by Joyce.  
%  
% This program will provide pressure amplitude and  
% the phase angle at the reciever. All distances are  
% ratios of dump distances Xc. All angles are inputed  
% in degrees. This model includes ArcTan Approximation  
% Reflection coefficient for fast bottom case and  
exponential  
% approximation for slow bottom case.  
%  
% By Pat Takamiya  
%  
clear; clc; clg;  
% Input Parameters  
B=input('Enter bottom wedge angle in deg (beta) =');  
G=input('Enter source angle from surface in deg (gamma) =');  
D=input('Enter receiver angle from surface in deg (delta)  
=');  
d1=input('Enter Density ratio, water to bottom =');  
CC=input('Enter sound speed ratio, water to bottom =');  
r1=input('Enter range of source from apex (r1) =');  
r2=input('Enter range of receiver from apex (r2) =');  
y0=0;  
%  
% Determine Number of Image Quadruplets  
% Convert Angles from Deg to Rads  
N1=fix(90/B);  
B=B*(pi/180);  
G=G*(pi/180);  
D=D*(pi/180);  
%  
% Determine Scaling for Fast or Slow Bottoms  
tqq=tan(B);  
    if CC<1                                % Fast Bottom  
        tqq1=acos(CC);  
        tqq2=sin(tqq1);  
    else  
        tqq1=acos(1/CC);    % Slow Bottom  
        tqq2=tan(tqq1);  
    end
```

```

tqq3=2*tqq2*tqq;
t4=pi/tqq3; % Scaled wave number
%
% Calculate Constants and Primary Doublet
%
alpha=2*(1/d1)/(sqrt((CC^2)-1));
r=sqrt((r1^2)+(r2^2)+(y0^2)-(2*r1*r2*cos(D)));
r3=abs(r2-r1);
r4=r1*r2/(r3^2);
mu=r2/r3;
q=t4*r1*G*D;
p1=(2/r)*sin(q);
f=0;
%
% Quadruplet Summation
%
n=(1:N1);
    s(n)=n;
    th(n)=2*n*B;
    d(n)=t4*r1*D*sin(th(n));
    phi(n)=t4*r1*mu*(1-cos(th(n)));
% Reflection Coeff
    ru(n)=sqrt((r1^2)+(r2^2)+(y0^2)-2*r1*r2*cos(th(n)+D));
    rl(n)=sqrt((r1^2)+(r2^2)+(y0^2)-2*r1*r2*cos(th(n)-D));
    r5(n)=r1./ru(n);
    r6(n)=r1./rl(n);
    a1(n)=1+r5(n).*cos(th(n));
    b1(n)=r6(n).*cos(th(n));
    if CC>1
        rr(n)=(B*alpha.*(n.^2));
        R(n)=-exp(-rr(n));
    else
        x(n)=sin(th(n))/sin(acos(CC));
        R1(n)=-exp(-2*j*atan((1/d1).*x(n))./sqrt(1-x(n).^2));
        R(n)=cumprod(R1(n));
    end
    a(n)=n.*alpha*D.*a1(n);
    b(n)=n.*alpha*G.*b1(n);
%
% Pressure
    u1(n)=cosh(b(n));
    u2(n)=exp(-j*phi(n));
    u3(n)=(-2/r).*R(n).*u1(n).*u2(n);
%
% Upper Image
    v1(n)=sin(th(n)+D);
    v2(n)=t4*r1*G*v1(n);

```

```

v3(n)=sin(v2(n));
v4(n)=cos(v2(n));
v5(n)=-a(n)-j*mu*d(n);
v6(n)=exp(v5(n));
v7(n)=tanh(b(n));
v8(n)=v6(n).*(v3(n)-j*v7(n).*v4(n));
%
% Lower Image
w1(n)=sin(th(n)-D);
w2(n)=t4*r1*G*w1(n);
w3(n)=sin(w2(n));
w4(n)=cos(w2(n));
w5(n)=a(n)+j*mu*d(n);
w6(n)=exp(w5(n));
w7(n)=w6(n).*(w3(n)-j.*v7(n).*w4(n));
%
% Summation
p(n)=u3(n).*(v8(n)-w7(n));
p2=sum(p(n));
%
%
ps=p1+p2;
ph1=atan2(imag(ps),real(ps));
phase=180*ph1/pi
P=sqrt(real(ps)^2 + imag(ps)^2)

```


APPENDIX B-1

```
%  
%  
% WEDGE for MATLAB  
%  
% Adapted from the BASIC version of WEDGE  
% by Prof A.B. Coppens and URTEXT by G. Nassopolous  
% pz Not Normalized  
%  
% This program will provide pressure amplitude and  
% the phase angle at the reciever. All distances are  
% ratios of dump distances Xc. All angles are inputed  
% in degrees. This model includes cross-slope and  
% bottomloss terms.  
%  
% By Pat Takamiya  
%  
clear; clc; clg;  
%  
B=input('Enter bottom wedge angle (beta)= ');  
G=input('Enter source angle from the surface (gamma)= ');  
D=input('Enter receiver angle from the surface (delta)= ');  
d1=input('Enter Density ratio, water to bottom= ');  
CC=input('Enter speed ratio, water to bottom= ');  
r1=input('Enter range of source from apex (r1)= ');  
r2=input('Enter range of receiver from apex (r2)= ');  
BL=input('Enter bottom loss coefficient (alpha/k2)= ');  
y0=input('Enter cross-slope range (Yo)= ');  
%  
% Determine Number of Image Pairs  
% Convert Angles from Deg to Rad  
%  
N1=fix(180/B);  
B=B*pi/180;  
G=B-G*pi/180;  
D=B-D*pi/180;  
%  
% Determine Scaling for Fast or Slow Bottom  
%  
tqq=tan(B);  
if CC<1, % Fast Bottom  
    tqql=acos(CC);  
    tqq2=sin(tqql);  
else
```

```

    tqql=acos(1/CC);          % Slow Bottom
    tqq2=tan(tqq1);
end;
%
% Determine Constants
%
tqq3=2*tqq2*tqq;
t4=pi/tqq3;
c2=CC^2;
d2=(r1^2)+(r2^2)+(y0^2);
r3=2*r1*r2;
q1=1/sqrt(2);
%
% Define Lengths of arrays
i=1:fix(N1/2);
c(i)=zeros(1:fix(N1/2));
e(i)=zeros(1:fix(N1/2));
f(i)=zeros(1:fix(N1/2));
%
% Determine Range to Receiver for each Image
%
    n=1:N1;
    n1=2:2:N1;
    n2=1:2:N1;
    t1(n1)=(n1*B)-G;
    t1(n2)=(n2-1)*B+G;
    r8(n)=sqrt(d2-r3*cos(t1(n)-D)); % 3-D Law of Cosines
    r9(n)=sqrt(d2-r3*cos(t1(n)+D)); % 3-D Law of Cosines

%
p1=0;p2=0;

for n=1:1:N1,
    s2=(-1)^(fix(n/2));

%
% Calculate Reflection Coefficient for Upper Space
%
    w1=2*c2*BL;
    i1=fix((n-1)/2);
    for i=1:1:i1,
        s(i)=(r1*sin(t1(n)-2*i*B)+r2*sin(2*i*B-D))/r8(n);
        if s(i)>=1,
            s(i)=1;
        end;
        c(i)=sqrt(1.0-s(i)^2);
        t=s(i)/d1;
    end
end

```

```

w0=-c2+c(i)^2;
y=sqrt((w0^2)+(w1^2));
z=(w0);
    if y<=z,
        y=z;
    end;
y1=q1*sqrt(y+w0);
y2=-q1*sqrt(y-w0);
z1=t-y2;
z2=-y1;
z3=z1/((z1^2)+(z2^2));
z4=-z2/((z1^2)+(z2^2));
z1=t+y2;
z2=y1;
z5=(z1*z3)-(z2*z4);
z6=(z1*z4)+(z2*z3);
e(i)=z5;
f(i)=z6;
end;
%
% Determine Pressure Contribution for the Upper Images
%
z1=0;z2=0;z3=0;z4=0;z5=1;z6=0;
    if n>2,
        for i=1:1:i1,
            z1=e(i);
            z2=f(i);
            z3=z5;
            z4=z6;
            z5=(z1*z3)-(z2*z4);
            z6=(z1*z4)+(z2*z3);
        end;
    end;
z1=z5;
z2=z6;
t=t4*r8(n);
z3=cos(t);
z4=-sin(t);
z5=(z1*z3)-(z2*z4);
z6=(z1*z4)+(z2*z3);
p1=p1+(s2*z5/r8(n));
p2=p2+(s2*z6/r8(n));
i1=i1+1;
%
% Determine Reflection Coefficient for the Lower Images
%
    for i=1:1:i1,

```

```

s(i)=(r1*sin(t1(n)-2*(i1)*B)+r2*sin(2*(i1)*B+D))/r9(n);
    if s(i)>1,
        s(i)=1;
    end;
c(i)=sqrt(1.0-s(i)^2);
t=s(i)/d1;
w0=-c2+c(i)^2;
y=sqrt((w0^2)+(w1^2));
z=(w0);
    if y<=z,
        y=z;
    end;
y1=q1*sqrt(y+w0);
y2=-q1*sqrt(y-w0);
z1=t-y2;
z2=-y1;
z3=z1/((z1^2)+(z2^2));
z4=-z2/((z1^2)+(z2^2));
z1=t+y2;
z2=y1;
z5=(z1*z3)-(z2*z4);
z6=(z1*z4)+(z2*z3);
e(i)=z5;
f(i)=z6;
end;
%
% Find Pressure Contribution for Lower Images
%
z1=0;z2=0;z3=0;z4=0;z5=1;z6=0;
    for i=1:1:i1,
        z1=e(i);
        z2=f(i);
        z3=z5;
        z4=z6;
        z5=(z1*z3)-(z2*z4);
        z6=(z2*z3)+(z1*z4);
    end;
z1=z5;
z2=z6;
t=t4*r9(n);
z3=cos(t);
z4=-sin(t);
z5=(z1*z3)-(z2*z4);
z6=(z2*z3)+(z1*z4);
p1=p1+(s2*z5/r9(n));
p2=p2+(s2*z6/r9(n));
end;

```

```

%
% Total Pressure at the Reciever
%
t5=sqrt(p1^2+p2^2)           % Pressure at Reciever
% Phase Angle at the Reciever
phaseang=atan2(p2,p1)*180/pi % Phase Angle

```

APPENDIX B-2

```

%
% WEDGE for MATLAB
%
% Adapted from the BASIC version of WEDGE
% by Prof A.B. Coppens and URTEXT by G. Nassopolous
% pz Not Normalized
%
% This program will provide pressure amplitude and
% the phase angle at the reciever. All distances are
% ratios of dump distances Xc. All angles are inputed
% in degrees. This model includes cross-slope,
% bottomloss, and is truncated at pz<0.00000001.
%
% By Pat Takamiya
%
clear; clc; clg;
%
B=input('Enter bottom wedge angle (beta)= ');
G=input('Enter source angle from the surface (gamma)= ');
D=input('Enter receiver angle from the surface (delta)= ');
d1=input('Enter Density ratio, water to bottom= ');
CC=input('Enter speed ratio, water to bottom= ');
r1=input('Enter range of source from apex (r1)= ');
r2=input('Enter range of receiver from apex (r2)= ');
BL=input('Enter bottom loss coefficient (alpha/k2)= ');
y0=input('Enter cross-slope range (Yo)= ');
%
% Determine Number of Image Pairs
% Convert Angles from Deg to Rad
%
N1=fix(180/B);
B=B*pi/180;
G=B-G*pi/180;
D=B-D*pi/180;
%
% Determine Scaling for Fast or Slow Bottom
%
tqq=tan(B);
if CC<1, % Fast Bottom
    tqq1=acos(CC);
    tqq2=sin(tqq1);
else
    tqq1=acos(1/CC); % Slow Bottom

```

```

    tqq2=tan(tqq1);
end;
%
% Determine Constants
%
tqq3=2*tqq2*tqq;
t4=pi/tqq3;
c2=CC^2;
d2=(r1^2)+(r2^2)+(y0^2);
r3=2*r1*r2;
q1=1/sqrt(2);
qa=1; % Truncation Tester
%
% Define Lengths of arrays
i=1:fix(N1/2);
c(i)=zeros(1:fix(N1/2));
e(i)=zeros(1:fix(N1/2));
f(i)=zeros(1:fix(N1/2));

%
% Determine Range to Receiver for each Image
%
n=1:N1;
n1=2:2:N1;
n2=1:2:N1;
t1(n1)=(n1*B)-G;
t1(n2)=(n2-1)*B)+G;
r8(n)=sqrt(d2-r3*cos(t1(n)-D)); % 3-D Law of Cosines
r9(n)=sqrt(d2-r3*cos(t1(n)+D)); % 3-D Law of Cosines

%
p1=0;p2=0;

for n=1:1:N1,
    s2=(-1)^(fix(n/2));

%
% Calculate Reflection Coefficient for Upper Space
%
w1=2*c2*BL;
i1=fix((n-1)/2);
for i=1:1:i1,
    s(i)=(r1*sin(t1(n)-2*i*B)+r2*sin(2*i*B-D))/r8(n);
    if s(i)>=1,
        s(i)=1;
    end;
    c(i)=sqrt(1.0-s(i)^2);

```

```

        t=s(i)/d1;
        w0=-c2+c(i)^2;
        y=sqrt((w0^2)+(w1^2));
        z=(w0);
        if y<=z,
            y=z;
        end;
        y1=q1*sqrt(y+w0);
        y2=-q1*sqrt(y-w0);
        z1=t-y2;
        z2=-y1;
        z3=z1/((z1^2)+(z2^2));
        z4=-z2/((z1^2)+(z2^2));
        z1=t+y2;
        z2=y1;
        z5=(z1*z3)-(z2*z4);
        z6=(z1*z4)+(z2*z3);
        e(i)=z5;
        f(i)=z6;
    end;

%
% Determine Pressure Contribution for the Upper Images
%
    z1=0;z2=0;z3=0;z4=0;z5=1;z6=0;
    if n>2,
        for i=1:1:i1,
            z1=e(i);
            z2=f(i);
            z3=z5;
            z4=z6;
            z5=(z1*z3)-(z2*z4);
            z6=(z1*z4)+(z2*z3);
        end;
    end;
    z1=z5;
    z2=z6;
    t=t4*r8(n);
    z3=cos(t);
    z4=-sin(t);
    z5=(z1*z3)-(z2*z4);
    z6=(z1*z4)+(z2*z3);
    p1=p1+(s2*z5/r8(n));
    p2=p2+(s2*z6/r8(n));
    i1=i1+1;

%
% Determine Reflection Coefficient for the Lower Images

```



```

%
for i=1:1:i1,
    s(i)=(r1*sin(t1(n)2*(i1)*B)+r2*sin(2*(i1)*B+D))/r9(n);
    if s(i)>1,
        s(i)=1;
    end;
    c(i)=sqrt(1.0-s(i)^2);
    t=s(i)/d1;
    w0=-c2+c(i)^2;
    y=sqrt((w0^2)+(w1^2));
    z=(w0);
    if y<=z,
        y=z;
    end;
    y1=q1*sqrt(y+w0);
    y2=-q1*sqrt(y-w0);
    z1=t-y2;
    z2=-y1;
    z3=z1/((z1^2)+(z2^2));
    z4=-z2/((z1^2)+(z2^2));
    z1=t+y2;
    z2=y1;
    z5=(z1*z3)-(z2*z4);
    z6=(z1*z4)+(z2*z3);
    e(i)=z5;
    f(i)=z6;
end;

%
% Find Pressure Contribution for Lower Images
%
z1=0;z2=0;z3=0;z4=0;z5=1;z6=0;
for i=1:1:i1,
    z1=e(i);
    z2=f(i);
    z3=z5;
    z4=z6;
    z5=(z1*z3)-(z2*z4);
    z6=(z2*z3)+(z1*z4);
end;
z1=z5;
z2=z6;
t=t4*r9(n);
z3=cos(t);
z4=-sin(t);
z5=(z1*z3)-(z2*z4);
z6=(z2*z3)+(z1*z4);
p1=p1+(s2*z5/r9(n));

```

```

        p2=p2+(s2*z6/r9(n));
% Truncation Test
        qa=qa*sqrt((z5*z5)+(z6*z6));
        if qa<0.00000001, break, end,
end;

%
% Total Pressure at the Reciever
%
t5=sqrt(p1^2+p2^2)           % Pressure at Reciever
% Phase Angle at the Reciever
phaseang=atan2(p2,p1)*180/pi % Phase Angle

```

LIST OF REFERENCES

1. Tappert, F. D., "The Parabolic Approximation Method", *Wave Propagation and Underwater Acoustics*, J. B. Keller and J. S. Papadakis, eds., Springer, 1977.
2. Collins, M. D., "Application and Time-domain Solution of Higher-Order Parabolic Equation in Underwater Acoustics", *J. Acoust. Soc. Am.*, **86**(3), September 1989.
3. Jensen, F. B. and Kuperman, W. A., "Sound Propagation in a Wedge-Shaped Ocean with a Penetrable Bottom", *J. Acoust. Soc. Am.*, **67**(5), May 1980.
4. Coppens, A. B. and Sanders, J. V., "Transmission of Sound into a Fast Fluid Bottom from an Overlying Fluid Wedge", *Proceedings of Workshop on Seismic Propagation in Shallow Water*, Office of Naval Research, Arlington, VA, 1978.
5. Lee, D. and McDaniel, S. T., "A Finite-Difference Treatment of Interface Conditions for the Parabolic Wave Equation: The Irregular Interface", *J. Acoust. Soc. Am.*, **73**(5), May 1983.
6. Collins, M. D., "The Rotated Parabolic Equation and Sloping Ocean Bottoms", *J. Acoust. Soc. Am.*, **87**(3), March 1990.
7. Fawcett, J. A., "Modeling Three-Dimensional Propagation in an Oceanic Wedge Using Parabolic Equation Methods", *J. Acoust. Soc. Am.*, **93**(5), May, 1993.
8. Thomson, D. J., "Wide-Angle Parabolic Equation Solutions to Two Range-Dependent Benchmark Problems", *J. Acoust. Soc. Am.*, **87**(4), April, 1990.
9. Collins, M. D., "An Energy-Conserving Parabolic Equation for Elastic Media", *J. Acoust. Soc. Am.*, **94**(2), August, 1993.
10. Collins, M. D. and Westwood, E. K., "A Higher Order Energy-Conserving Parabolic Equation for Range-Independent Ocean Depth, Sound Speed, and Density", *J. Acoust. Soc. Am.*, **89**(3), March, 1991.
11. Coppens, A. B., Frey, A. R., Kinsler, L. E., and Sanders, J. V., *Fundamentals of Acoustics, Third Edition*, p.430,432,114, John Wiley & Sons, Inc., Monterey, CA, 1980.
12. Pierce, A. D., "Extension of the Method of Normal Modes to Sound Propagation in an Almost-Stratified Medium", *J. Acoust. Soc. Am.*, **36**(1), January 1965.
13. Graves, R. D., Nagl, A., Uberall, H., and Zarur, G. L., "Range-Dependent Normal Modes in Underwater Sound Propagation: Application to the Wedge Shaped Ocean", *J. Acoust. Soc. Am.*, **58**(6), December 1975.

14. Buckingham, M. J., "Theory of Three-Dimensional Acoustic Propagation in a Wedgelike Ocean with a Penetrable Bottom", *J. Acoust. Soc. Am.*, **82**(1), July 1987.
15. Pierce, A. D., "Augmented Adiabatic Mode Theory for Upslope Propagation from a Point Source in a Variable-Depth Shallow Water Overlying a Fluid Bottom", *J. Acoust. Soc. Am.*, **74**(6), December 1983.
16. Arnold, J. M. and Felsen, L. B. "Intrinsic Modes in a Nonseparable Ocean Waveguide", *J. Acoust. Soc. Am.*, **76**(3), September 1984.
17. Macpherson, J. D. and Daintith, M. J., "Practical Model of Shallow Water Acoustic Propagation", *J. Acoust. Soc. Am.*, **41**(4), 1966.
18. Kawamura, M., Ioannou, G., *Pressure on the Interface Between a Converging Fluid Wedge and a Fast Fluid Bottom.*, Master's Thesis, Naval Postgraduate School, Monterey, CA, December 1978.
19. Coppens, A. B., Humphries, M., Sanders, J. V., "Propagation of Sound out of a Fluid Wedge into an Underlying Fluid Substrate of Greater Sound Speed", *J. Acoust. Soc. Am.*, **76**(5), November 1984.
20. Brekhovskikh, L. and Lysanov, Y., *Fundamentals of Ocean Acoustics*, Springer-Verlag, New York; 1982.
21. Baek, C., *The Acoustic Pressure in a Wedge-Shaped Water Layer Overlying a Fast Fluid Bottom*, Master's Thesis, Naval Postgraduate School, Monterey, CA, March 1984.
22. LeSesne, P. K., *Development of Computer Programs Using the Method of Images to Predict the Sound Field in a Wedge Overlaying a Fast Fluid and Comparison with Laboratory Experiments*, Master's Thesis, Naval Postgraduate School, Monterey, CA, December 1984.
23. Kosnick, M.E., *The Implicit Finite-Difference (IFD) Acoustic Model in a Shallow Water Environment*, Master's Thesis, Naval Postgraduate School, Monterey, CA, June 1984.
24. Kaswandi, C., *A Computerized Investigation Using the Method of Images to Predict the Sound Field in a Fluid Wedge Overlaying a Slow Half-Space*, Master's Thesis, Naval Postgraduate School, Monterey, CA, December 1987.
25. Nassopoulos, G., *Study of Sound Propagation in a Wedge Shaped Ocean and Comparison with Other Methods*, Master's Thesis, Naval Postgraduate School, Monterey, CA, June 1992.

26. Livingood, D. M., *Extension of the Analytical Approximation to the Transmission of Sound in Shallow Water Using the Image Model*, Master's Thesis, Naval Postgraduate School, Monterey, CA, September 1992.
27. Joyce, M. D., *Quadruplet Expansion of the Acoustic Pressure Field in a Wedge Shaped Ocean*, Master's Thesis, Naval Postgraduate School, Monterey, CA, September 1993.
28. Coppens, A.B., *Personal Notes*, Naval Postgraduate School, Monterey, CA, August 1993-March 1994.
29. Urick, R.J., *Principles of Underwater Sound*, 3rd Edition, p.139, McGraw-Hill, Inc, New York, 1983.
30. Thomas, G.B., Finney, R.L., *Calculus, Revised Printing*, p.641, Addison-Wesley Publishing Company, Menlo Park, CA, 1991.
31. Math Works, Inc., *The Student Edition of MATLAB™*, Prentice Hall, Inc., Englewood Cliffs, New Jersey, 07632.

BIBLIOGRAPHY

Ansbrosio, A. P. and Arnold, J. M., "Numerically Efficient Evaluation of Intrinsic Modes in Wedge-Shaped Waveguides", *J. Acoust. Soc. Am.*, **89**(4), April, 1991.

Arnold, J. M. and Felsen, L. B., "Rays and Local Modes in a Wedge-shaped Ocean", *J. Acoust. Soc. Am.*, **73**(4), April 1983.

Bradshaw, N., *Propagation of Sound in a Fast Bottom Underlying a Wedge-Shaped Medium*, Master's Thesis, Naval Postgraduate School, Monterey, CA, September, 1980.

Buckingham, M. J., *Acoustic Propagation in a Wedge Shaped Ocean with Perfectly Reflecting Boundaries*, NATO Advanced Research Workshop on a Hybrid Formulation of Wave Propagation and Scattering, 1983.

Buckingham, M. J., *Acoustic Propagation in a Wedge Shaped Ocean*, The A. B. Wood Memorial Lecture, Naval Research Lab, 1967 .

Buckingham, M. J., *Acoustic Propagation in a Wedge-Shaped Ocean with Perfectly Reflecting Boundaries*, Naval Research Laboratory Report 8797, 1984.

Buckingham, M. J., and Tolstoy, A., "An Analytical Solution for Benchmark Problem 1: The 'Ideal' Wedge", *J. Acoust. Soc. Am.*, **87**(4), April 1990.

Collins, M. D. and Chin-Bing, S. A. "A Three-Dimensional Parabolic Model that Includes the Effects of Rough Boundries", *J. Acoust. Soc. Am.*, **87**(3), March, 1990.

Collins, M. D., "Benchmark Calculations for Higher-Order Parabolic Equations", *J. Acoust. Soc. Am.*, **87**(4), April 1990.

Collins, M. D., "High Order Parabolic Approximation for Accurate and Stable Elastic Parabolic Equation with Applications to Interface Wave Propagation", *J. Acoust. Soc. Am.*, **89**(3), March, 1991.

Collins, M. D. and Westwood, E. K., "A Higher Order Energy-Conserving Parabolic Equation for Range-Independent Ocean Depth, Sound Speed, and Density", *J. Acoust. Soc. Am.*, **89**(3), March, 1991.

Collins, M. D., "A Two-Way Parabolic Equation for Elastic Media", *J. Acoust. Soc. Am.*, **93**(4), April, 1993.

Collins, M. D., "An Energy-Conserving Parabolic Equation for Elastic Media", *J. Acoust. Soc. Am.*, **94**(2), August, 1993.

Deane, G. B. and Buckingham, M. J., "An Analysis of the Three-dimensional Sound Field in a Penetrable Wedge with a Stratified Fluid or Elastic Basement", *J. Acoust. Soc. Am.*, **93**(3), March 1993.

Deane, G. B. and Tindle, C. T., "A Three Dimensional Analysis of Acoustic Propagation in a Penetrable Wedge Slice", *J. Acoust. Soc. Am.*, **92**(3), September 1992.

Desaubies, Y., Chiu, C.S., Miller, J., "Acoustic Mode Propagation in a Range-dependent Ocean", *J. Acoust. Soc. Am.*, **80**(4), 1986.

Evans, R. B., "A Coupled Mode Solution for Acoustic Propagation in a Waveguide with Stepwise Depth Variation of a Penetrable Bottom", *J. Acoust. Soc. Am.*, **74**(1), July 1983.

Evans, R.B., "The Decoupling of Stepwise Coupled Modes", *J. Acoust. Soc. Am.*, **80**(5), 1986.

Felson, L. B., "Benchmarks: An Option for Quality Assessment", *J. Acoust. Soc. Am.*, **87**(4), April 1990.

Green, R. R., "The Rational Approximation to the Acoustic Wave Equation with Bottom Interaction", *J. Acoust. Soc. Am.*, **76**(6), December 1984.

Jaeger, L.E., *A Computer Program for Solving the Parabolic Equation Using an Implicit Finite-difference Solution Method Incorporating Exact Interface Conditions*, Master's Thesis, Naval Postgraduate School, Monterey, CA, 1983.

Jensen, F. B., Tindle, C. T., "Numerical Modeling Results for Mode Propagation in a Wedge", *J. Acoust. Soc. Am.*, **82**(1), July 1987.

Kamal, A., and Felson, L. B., "Spectral Theory of Sound Propagation in an Ocean Channel with Weakly Sloping Bottom," *J. Acoust. Soc. Am.*, **73**(4), April 1983.

Kim, J.R., *Comparison of Sound Pressure in a Wedge Shaped Ocean as Predicted by an Image Method and a PE Model*, Master's Thesis, Naval Postgraduate School, Monterey, CA, December 1990.

Kuznetsov, V. K., "Method of Virtual Sources in the Underwater Acoustical Description of High-Frequency Sound Field in a Wedge", *Soviet Physical Acoustics*, **18**(2), 1972.

Lian S. W. and Pace, N. G., "Evaluations of the Analytic Solution for the Acoustic Field in an Ideal Wedge and the Approximate Solution in a Penetrable Wedge", *J. Acoust. Soc. Am.*, **89**(1), 1991.

McDaniel, S. T., "Mode Coupling Due to Interaction with the Seabed", *J. Acoust. Soc. Am.*, **72**(3), 1982.

Meisenheimer, C. C., *A Comparison of Two Computer Models of Sound Propagation for a Wedge Shaped Ocean Over a Penetrable Bottom*, Master's Thesis, Naval Postgraduate School, Monterey, CA, September 1993.

Nagl, A., Uberall, H., Haug, A. J., and Zarur, G. L., "Adiabatic Mode Theory of Underwater Sound Propagation in a Range-Dependent Environment", *J. Acoust. Soc. Am.*, **63**(3), 1978.

Paliatsos, D., *Computer Studies of Sound Propagation in a Wedge-Shaped Ocean with Penetrable Bottom*, Master's Thesis, Naval Postgraduate School, Monterey, CA, March 1989.

Pierce, A. D., "Guided Mode Disappearance During Upslope Propagation in Variable Depth Shallow Water Overlying a Fluid Bottom", *J. Acoust. Soc. Am.*, **72**(2), 1982.

Plumpton, N. G., and Tindle, C. T., "Saddle Point Analysis of the Reflected Acoustic Field", *J. Acoust. Soc. Am.*, **85**, 1989.

Sagos, G. A., *A Three-Dimensional Coupled Normal Mode Model for Sound Propagation in Shallow Water with Irregular Bottom Bathymetry*, Master's Thesis, Naval Postgraduate School, Monterey, CA, December 1992.

Westwood, E. K., "Ray Model Solutions to the Benchmark Wedge Problems", *J. Acoust. Soc. Am.*, **87**(4), April 1990.

INITIAL DISTRIBUTION LIST

		No. Copies
1.	Defense Technical Information Center Cameron Station Alexandria, VA 22304-6145	2
2.	Library, Code 52 Naval Postgraduate School Monterey, CA 93943-5002	2
3.	Director, Submarine Warfare Division (N87) Chief of Naval Operations Pentagon Room 4E453 Navy Department Washington, DC 20350-2000	1
4.	Director, Expeditionary Warfare Division Chief of Naval Operations (N85) Pentagon Room 4A720 Navy Department Washington, DC 20350-2000	1
5.	Dr. A. B. Coppens, Code PH/Cz Department of Physics Naval Postgraduate School Monterey, CA 93943-5002	2
6.	Dr. J. V. Sanders, Code PH/Sd Department of Physics Naval Postgraduate School Monterey, CA 93943-5002	2
7.	LT P.T. Takamiya 1501 Akialoa Way Kailua, HI 96734	3
8.	Dr. David Kast 1184 Hilby Ave. Seaside, CA 93955	1